The effects of a soluble surfactant on the interfacial dynamics of stationary bubbles in inclined tubes

By DANIEL P. CAVANAGH[1] AND DAVID M. ECKMANN[2]

[1]Biomedical Engineering Program and Department of Chemical Engineering, Bucknell University, Lewisburg, PA 17837, USA

[2]Department of Anesthesia and The Institute for Medicine and Engineering, University of Pennsylvania, Philadelphia, PA 19104, USA

We have experimentally examined the effects of a common soluble surfactant on gas bubbles in liquid flows in inclined tubes. Air bubbles of known size ($\lambda = 0.8, 1.0, 1.5$) are held stationary under minimum flow conditions in tubes inclined at fixed angles ($\omega = 25°, 45°, 65°, 90°$). Sodium dodecyl sulphate (SDS) is infused into the bulk flow at two bulk concentrations ($C = 10\%$ or 100% critical micelle concentration (CMC)). In addition to recording pressure and flow waveforms, we capture video images of bubbles before and during exposure to the surfactant. Modification of the interfacial properties by the surfactant results in extremely dynamic bubble behaviour including interfacial deformation, deformation plus axial translation, and bubble detachment from the wall plus translation. We measure the corresponding time-dependent pressure gradient within the tube. The surfactant mediated responses observed are dependent upon the interrelated effects of C, λ and ω. A high bulk concentration of surfactant may produce more rapid modification of bubble shape and influence wetting, thus increasing the potential for bubble detachment. The likelihood that detachment will occur increases further as bubble volume in increased. In both vertical tubes in which contact forces are absent and in non-vertical tubes, the infusion of surfactant may result in axial translation either in the direction of, or opposite to, the direction of the bulk flow. Critical to the translation and/or detachment of the bubble is the surfactant-mediated modification of contact line mechanics. Contact line velocities corresponding to rates of shrinkage of dewetted surface area are extracted from experimental data. We also explore the potential effects of surfactants on interfacial remobilization. This investigation demonstrates the potential use of surfactants to be used for dislodging dewetted gas bubbles by the intentional manipulation of interfacial properties.

1. Introduction

The interfacial dynamics associated with a gas bubble trapped within a liquid flow have been of great interest to a variety of workers in fields ranging from oil recovery to cardiopulmonary medicine (Branger & Eckmann 1999, 2002). We have previously reported on an experimental investigation that produced video images of gas bubbles dewetted onto glass and acrylic tube walls (Cavanagh & Eckmann 1999). This dewetting phenomenon acted as a motion resistant force which held the bubbles stationary over a range of bulk flow rates at various tube angles. In the current

experimental investigation, we explore the effects of a soluble surfactant infused into the bulk flow to alter the interfacial mechanics of stationary bubbles and promote their detachment from acrylic tubes.

Cavanagh & Eckmann (1999) provides a detailed description of past investigations into the mechanics of gas bubbles and liquid drops in liquid flows. The current investigation uses similar dimensionless parameters in order to evaluate the relative contributions of the predominant mechanical forces. The first is a geometric parameter, $\lambda = a/d$, which provides a dimensionless measure of bubble size in which a is the diameter of the undisturbed spherical volume of the bubble ($V_{bubble} = \frac{1}{6}\pi a^3$) and d is the inner diameter of the tube. The Reynolds number, $Re = U_b d\rho_b/\mu_b$ (U_b, bulk fluid mean velocity; ρ_b, bulk fluid density; μ_b, bulk fluid viscosity), relates the importance of the inertial forces to the viscous forces while the Froude number, $Fr = U_b/(gd)^{1/2}$ (g, acceleration due to gravity), provides a comparison of the inertial to the gravitational forces. As demonstrated by Maxworthy (1991), Fr may be expressed as $Fr_\omega = U_b/(gas\ in\ \omega)^{1/2}$ which incorporates both the tube inclination (ω) and bubble volume. The Bond number, $G = \Delta\rho g d^2/\gamma$ ($\Delta\rho$, density difference; γ, surface tension), and the capillary number, $Ca = \mu_b U_b/\gamma$, provide the relative importance of gravitational and viscous forces to surface tension forces, respectively. The Weber number, $We = \rho_b U_b^2 d/\gamma = CaRe$, is frequently used to present the ratio of inertial to surface tension forces. The dimensionless viscosity parameter, $\eta = \mu/\mu_b$, is a ratio of the bubble (or drop) viscosity to that of the bulk fluid.

For investigations including the effects of surfactants, additional dimensionless parameters become important. The bulk Péclet number, $Pe_b = U_b d/D_b$ (D_b, diffusivity of surfactant in bulk fluid) relates the contributions of convectional transport and diffusional transport within the bulk fluid phase. A surface Péclet number may also be defined as $Pe_s = U_b d/D_s$ (D_s, diffusivity of surfactant on the air–water interface). In general, D_s may be approximated to be of order $10^{-6}\ \mathrm{m^2\,s^{-1}}$ (Chen & Stebe 1997). The Biot number, $Bi = \alpha d/U_b$ (α, desorption rate constant) is frequently used to relate the rates of kinetic desorption of the surfactant from the interface and surface convection. Finally, the scaled form of the bulk concentration of surfactant may be given as $k = \beta C/\alpha$ (β, adsorption rate constant; C, bulk surfactant concentration far from the bubble). The two parameters Bi and k are similar to those used in Fdhila & Duineveld (1996) and Wang, Papageorgiou & Maldarelli (1999).

The addition of a surfactant to the clean interfacial experiments described in Cavanagh & Eckmann (1999) will cause modification of interfacial properties at the gas–liquid interface as well as along the contact line where all three phases (gas, liquid and solid) meet. Background information relevant to both clean and surfactant-laden interfaces is therefore provided. Since much of the relevant background literature focuses on bubbles or drops moving through infinite media, we include these investigations to provide insight for interpreting the current results.

Levich (1962) provided early documentation on the effects of surfactants on the interface of a bubble. This work describes the effects of surfactants that adsorb to a rising gas bubble and are convected to the rear of the bubble, thereby inducing a non-uniform distribution of surfactant along the interface. This non-uniform distribution leads to the development of surface tension gradients which retard bubble surface motion and increase drag on the bubble. This investigation has motivated many workers to explore further the dynamic effects of surfactants on gas–liquid interfaces.

Davis & Acrivos (1966) numerically modelled the development of surface tension gradients on a bubble creeping through a fluid containing trace amounts of a surfactant. Levan & Newman (1976) used numerical methods to show that the terminal

velocity of a rising bubble is decreased and that the gas–liquid interfacial velocity is decreased if trace amounts of surfactant are present in the bulk liquid phase. Yamamoto & Ishi (1987) experimentally measured the effects of surfactants on the shape and rise velocities of large rising gas bubbles. Whereas the rising velocities were scarcely influenced, the drag coefficients of the bubbles were influenced by minute amounts of surfactants. Park (1992) examined the motion of a finite length bubble in the presence of a small amount of surfactant in the limit of small Ca. He found that the pressure required to drive the bubble through a capillary tube increases linearly with the length of the bubble up to a critical bubble length beyond which the pressure remains constant.

Fdhila & Duineveld (1996) performed experiments and simulations of small, spherical bubbles ($d \sim O(1\,\text{mm})$) rising in an infinite medium containing surfactants. For $Pe \sim O(10^5)$, surfactant molecules adsorb to the interface and are convected to the rear of the bubble where a stagnant cap forms. This process decreases the bubble rise velocity. Their numerical analysis assumed no bubble deformation and that the surfactant exchange was governed by sorption mechanics, as adsorption was much slower than diffusion. As an extension of these concepts, Wang *et al.* (1999) concluded from their theoretical approach that a bubble with decreased rise velocity owing to surface surfactant concentration gradients may have its mobility increased through raising the bulk concentration of surfactant. For high Pe_b, large bulk concentrations are required to remobilize the bubble surface completely. Also provided in their manuscript is an excellent review of the literature addressing the two different regimes of surfactant transport. The first of these is described as the insoluble regime in which the rate of convection of surfactant on the interface is much greater than the rates of bulk diffusion or kinetic exchange. In the second regime, the convection rate is of the same order as the bulk diffusion and kinetic exchange so that the transport in the bulk phase is significant. It is in this regime that the authors determine that the surface can be remobilized at high enough bulk concentrations of surfactant.

Liao & McLaughlin (2000) numerically simulated the unsteady motion of a single bubble ($d \sim O(1\,\text{mm})$) to evaluate the effects of surfactants on bubble motion and shape. For low bulk concentrations of surfactants, they report the formation of the commonly observed immobilized surfactant cap at the rear of the bubble. They also found that the adsorption rate constant has a significant effect on bubble rise velocities. Zhang & Finch (2001) experimentally examined the rise of single bubbles in surfactant solutions and found that the steady rise velocity is independent of surfactant concentration for a range of concentrations below the critical micelle concentration. DeBisschop, Miksis & Eckmann (2002) modelled a two-dimensional bubble rising in an inclined channel in the presence of an insoluble surfactant. They determined that the bubble velocity increased with increasing G, and bubble dimensions as a function of G compared well to measurements made by Cavanagh & Eckmann (1999).

For additional insight into our investigation, we also include a brief summary of some prior work that has focused on the effects of surfactants on liquid drops. Flumerfelt (1980) used a numerical approach to analyse the effects of dynamic interfacial properties on drop deformation and orientation. This investigation is limited by assumptions of linear bulk/interface transport of surfactant and small variations of surfactant on the interface. A related experimental investigation by Phillips, Graves & Flumerfelt (1980) provided results that agreed well with Flumerfelt's (1980) findings. Only in systems with extremely high bulk viscosities was the effect of dynamic interfacial properties found to be negligible. Oguz & Sadhal (1988) numerically examined

the fluid dynamics of moving drops in the presence of a soluble surfactant. Their results were in good agreement with previous experiments at $Pe_b \sim 700$.

In two separate investigations, Zhang & Basaran (1995, 1997) examined the effects of soluble surfactants on drop formation and drop impact with a hard surface, respectively. In the first investigation, they found that effects of surfactants on drop formation were strongly dependent upon the rates of interfacial dilation and surfactant transport. In the subsequent paper, they discuss the competition between surfactant enhanced interfacial spreading and the spreading inhibiting the development of Marangoni stresses in controlling droplet spreading with surfactant present. The Marangoni stresses were also examined by Pawar & Stebe (1996) whose theory focused on the effects of insoluble surfactants on drop deformation in an extensional flow.

The direct effects of surfactants on drop deformation and breakup were numerically examined by Stone & Leal (1990) for extensional flows with low Reynolds numbers. They determined that at low Ca the presence of surfactant causes more severe deformation than that observed in a surfactant free system. At large Ca, the surfactant transport competes with the dilution of the surfactant due to increasing interfacial area. Stone (1990) also provides a derivation of the time-dependent convective diffusion equation for surfactant transport along a deforming interface.

In separate numerical studies of the motion of drops in circular tubes in the presence of bulk insoluble surfactants, He, Dagan & Maldarelli (1991) and Borhan & Mao (1992) observed the development of surface tension gradients (and hence, Marangoni stresses) that opposed surface convection and retarded drop motion. Borhan & Mao (1992) also found that for large Pe_s, the Marangoni stresses immobilize the surface, resulting in a significant increase in the pressure gradient required to transport the drop through the tube. They also studied the coupled effects of: (i) local increases of interfacial curvature in response to reduction of surface tension, and (ii) an increase in interfacial area stemming from drop deformation, but resulting in a decreased surfactant concentration on the interface.

Stebe, Lin & Maldarelli (1991) experimentally and theoretically demonstrated the remobilization of drop surfaces containing adsorbed surfactants when the desorption kinetics and bulk diffusion mechanics are fast relative to the convective transport of surfactant on the interface. This prevents the development of a non-uniform surfactant distribution on the interface. Subsequently, Stebe & Maldarelli (1994) explored the use of specific surfactants for remobilizing interfaces that were previously immobilized with a separate surfactant. Through controlling the bulk concentration of the remobilizing surfactant, they investigated a range of interfacial stress conditions ranging from stress-free to significant interfacial retardation. Chen & Stebe (1996) further evaluated numerically the phenomena of surface remobilization, focusing on the effects of Marangoni retardation on the terminal velocity of a settling droplet. They explored both the Langmuir and the Frumkin nonlinear adsorption frameworks in their analysis of the surfactant exchange mechanics. Chen & Stebe (1997) then investigated the surfactant-induced retardation of the thermocapillary migration of a droplet where surface remobilization may occur for high bulk surfactant concentrations (i.e. large k) if adsorption–desorption rates are fast compared to the surface convective flux (i.e. $Bi \rightarrow \infty$). In this investigation, they included the energy barriers to surfactant adsorption and desorption in their definition of k and Bi. Johnson & Borhan (1999) consider the effects of a confining tube in their numerical analysis of the effects of insoluble surfactants on the motion of a drop under low-Reynolds-number conditions. Using the Frumkin adsorption framework,
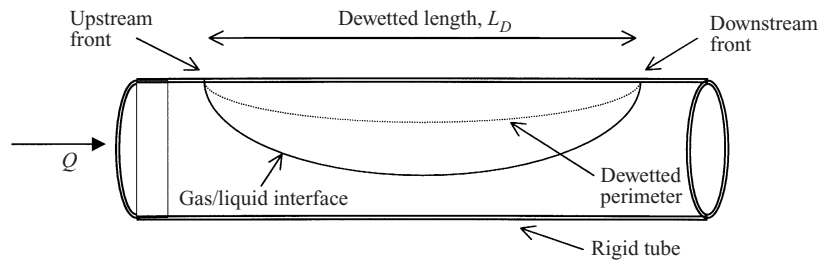
FIGURE 1. Dewetted bubble depiction.

they explore the significance of non-ideal surfactant interactions. They also examined the evolution of the shape of a bubble translating at low Reynolds number through a surfactant-containing unbounded liquid (Johnson & Borhan 2000).

Relevant to all of these studies involving surfactant transport is the adsorption dynamics of surfactants on gas–liquid interfaces. A comprehensive review of the transport kinetics is provided in Chang & Franses (1995). Many models of surfactant adsorption–desorption kinetics are reviewed, including the modified Langmuir–Hinshelwood (MLH) kinetic model which best describes the adsorption–desorption kinetics of sodium dodecyl sulphate (SDS), the surfactant used in the current experiments. The MLH model describes the mixed-kinetic, or adsorption limited, behaviour of SDS. It includes the adsorption and desorption energy barriers and the ability of the surfactant monolayer to capture additional surfactant molecules. The MLH model correlates well with experimental data, but one of its disadvantages is that the adsorption and desorption rate constants vary with bulk surfactant concentration.

Although the many studies cited above provide insight into the possible modes of surfactant transport mechanics, they do not incorporate the contact line mechanics that are potentially important in the current experiments. As shown in Cavanagh & Eckmann (1999), bubbles in tubes of diameter $d \sim 0.6$ cm do not occupy the entire cross-sectional area of the tube to form an airlock. Instead, a dewetted perimeter where all three phases meet may form, displaying two distinct contact fronts, i.e. the upstream and downstream fronts (see figure 1). These fronts may alternate between advancing and receding depending upon the direction of flow and bubble motion. Therefore, the relevant forces involved in this experimental system will be the buoyancy force of the bubble, the drag forces derived from the bulk flow, and the adhesion forces derived from surface tension acting around the contact perimeter. For a stationary dewetted bubble in the flow in a cylindrical tube, an appropriate expression for the overall force balance can be proposed similar to those found in Blackmore, Li & Gao (2001), Dussan V. (1987) and Dussan V. & Chow (1983). Whereas the latter two papers discuss the important forces on a liquid drop adhering to a solid surface under the effects of gravity or surrounding fluid motion, Blackmore *et al.* provide a balance of forces on bubbles exposed to shear flows in slit microchannels. For a stationary bubble (i.e. no axial bubble motion) in the current experimental system, the drag force on the bubble owing to bulk fluid motion must balance the adhesion force around the contact perimeter and the buoyancy force on the bubble. The drag force may be divided into separate pressure and viscous drag forces since the bulk fluid velocities are significant, which was not the case for Blackmore *et al.* who did not consider viscous drag. This axial force balance may be

expressed in cylindrical coordinates as:

$$(\Delta P_{bubble})A_z + \underset{surface}{\iint} \tau(\mu, \boldsymbol{U}(R,\theta,z))\,\mathrm{d}A$$

$$= \int_l \gamma(R,\theta,z)\cos(\phi(R,\theta,z))\,\mathrm{d}l + \Delta\rho g V_{bubble}\sin\omega. \quad (1)$$

In (1), ΔP_{bubble} is the axial pressure drop across the bubble, A_z is the projection of the cross-sectional area of the bubble in the radial plane, τ is shear stress, $\boldsymbol{U}$ is the velocity vector, γ is the surface tension, and ϕ is the contact angle in the liquid phase. The two terms on the left-hand side are the pressure and viscous drag terms, respectively, with the viscous form stemming from common fluid mechanics definitions of viscous drag. For large bubbles with surfactant-free interfaces, the viscous term is expected to be negligible in the overall force balance (Cavanagh & Eckmann 1999). The sum of these two drag forces is equal to the sum of the contact force integrated around the contact perimeter and the buoyancy force for inclination angle ω.

Note that in this complicated three-dimensional problem, τ, γ and ϕ may vary spatially along the interfaces of interest. As the buoyancy force remains constant for fixed V_{bubble} and ω, disruption of the stationary state could be induced through a modification of either the drag or adhesion forces. This static force balance suggests that an important concept in bubble dislodgment might be found in the alteration of the interfacial tension at the gas–liquid interface. As the contact angle is not necessarily directly related to the gas–liquid interfacial tension, the adhesion force which depends on the product $\gamma\cos\phi$ is of great interest in this problem. The exact effect of a surfactant on the force balance in (1) will be highly dependent on the interrelationship between the surfactant's effects on surface tension and contact angle. An experimental analysis of the behaviour of $\gamma\cos\phi$, termed the adhesion tension, has recently been published by Eckmann, Cavanagh & Branger (2001). They determined that the adhesion tension generally increases and then plateaus as surfactant concentration increases. In addition to modifying the adhesion term, the alteration of γ may also modify the geometry of the gas–liquid interface leading to a modification of A_z and hence, a modification of the drag force. Finally, the adsorption of surfactant at a gas–liquid interface may alter the viscous drag force through the development of Marangoni stresses. It becomes evident that addition of a surfactant to the flow may disturb the static force balance by altering either the adhesion or drag forces or both.

For additional insight into past investigations involving the effects of surfactants on contact line mechanics, we include here a brief review of some relevant literature. Numerous authors have examined the behaviour of liquid drops on solid surfaces in various orientations (Furmidge 1962; Dussan V. & Chow 1983; Dussan V. 1985; Milinazzo & Shinbrot 1988; Iliev 1997). Yon & Pozrikidis (1999) numerically examined the effects of an insoluble surfactant on the deformation of a liquid drop adhering to a plane wall. The behaviour of liquid drops exposed to a moving external fluid has also been extensively examined (Dussan V. 1987; Durbin 1988; Li & Pozrikidis 1996; Dimitrakopoulos & Higdon 1997, 1998). Durbin (1988) also provides an analysis of the flow separation that can occur on the downstream side of a liquid drop exposed to a wind force. In their numerical investigation of flow-induced displacement of a two-dimensional droplet adhering to a wall, Schleizer & Bonnecaze (1999) examined the effects of surfactants on the droplet behaviour. In the analysis, the surfactant was convected to the rear of the drop, thereby establishing Marangoni stresses which

immobilize the interface and reduce deformation. The analysis also permits movement of the contact edges along the solid boundary. One important finding is that the upstream and downstream contact edges do not translate at the same velocity. Therefore, the distance between the two points, termed the contact length, may either elongate or shorten, depending on simulation conditions including values of ϕ, Ca and η. Also, they mention the potential for the contact length to shrink to zero resulting in a detached droplet. In their investigation, the surfactant is not soluble in the bulk phase and therefore cannot be transported to or from the bulk fluid.

For systems in which the bubble partially occludes the flow path, dislodgement of the bubble involves translation along the tube wall and/or detachment from the wall. Bubble detachment is defined as the process in which the air–tube interface, or dewetted area, decreases in size to zero. Detachment of the bubble from the wall will be controlled by the forces acting upon the bubble. The net adhesion force around the dewetted contact perimeter keeps the bubble in place in opposition to any other forces such as buoyancy- and the flow-derived drag forces. As illustrated by (1), for a static bubble in a stagnant fluid, detachment will be determined by the relative strength of the buoyancy and surface tension derived adhesion forces. Under an imposed flow, the additional drag forces complicate the system further. Any attempt to dislodge or detach the bubble from a surface will require a modification of the force balance. An understanding of the effects of surfactants on the relevant forces acting on stationary bubbles is the major focus of this work.

This paper is divided in four sections. This section has presented the motivation for the investigation in addition to relevant background information. Section 2 provides a brief description of the experimental apparatus (§ 2.1), the experimental procedure (§ 2.2), and the image analysis techniques (§ 2.3). The results of the experiments with corresponding discussion are presented in § 3 as analysis of surfactant transport regimes (§ 3.1), overall bubble response to surfactants (§ 3.2), pressure difference modifications (§ 3.3) and contact edge velocity analysis (§ 3.4). Our conclusions are presented in § 4.

2. Experimental methods

2.1. *Experimental apparatus*

The apparatus used in the current experimental investigation is shown in figure 2 and is a modified version of that described in Cavanagh & Eckmann (1999). A general overview of the system is provided in addition to a detailed description of the modifications made for the current investigation. For a detailed description, see Cavanagh & Eckmann (1999).

For this investigation, the test section consists of a 64 cm long, rigid acrylic tube (i.d. = 0.635 cm) with tube couplers attached at either end to allow pressure gradient monitoring. This test section is mounted on a custom inclination platform allowing the test section to be maintained at inclination angles of $\omega = 0°$ (horizontal) to $\omega = 90°$ (vertical). The entire platform is positioned on top of a custom vibration isolation platform. A CCD camera (Javelin Ultrachip high resolution) mounted on an X, Y traversing table (Arrick Robotics) allows for visualization at any point along the axis of the test section. A mirror reflecting the top view of the test section into the camera field has been incorporated into the apparatus which allows the operator to record the side and top views simultaneously with one camera (see figure 3). Video images are recorded using a videorecorder (Sony SVO-9500 ND) for
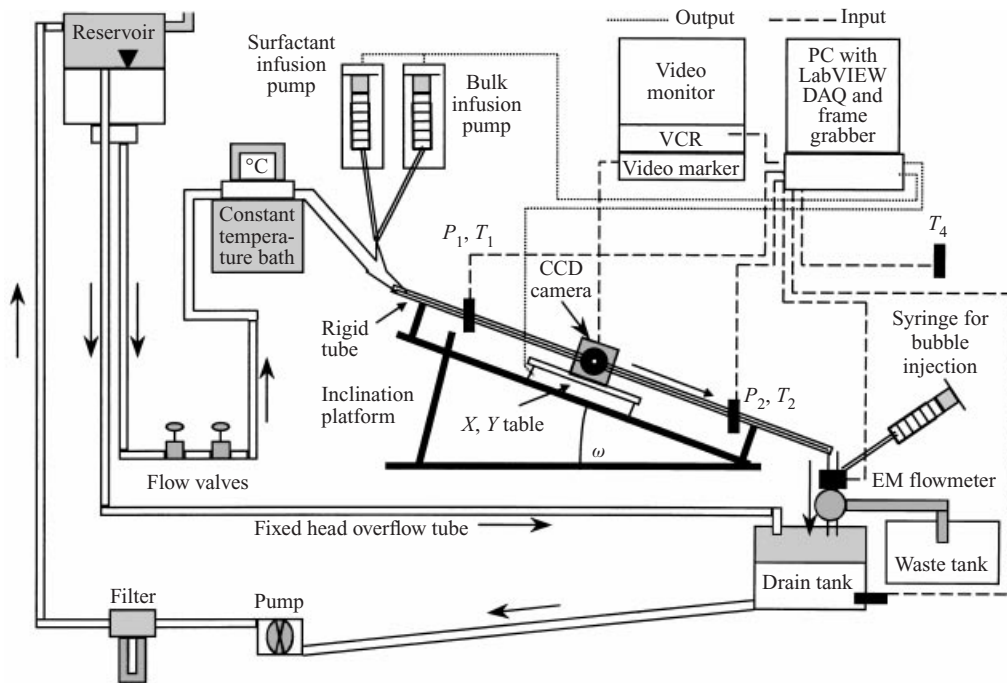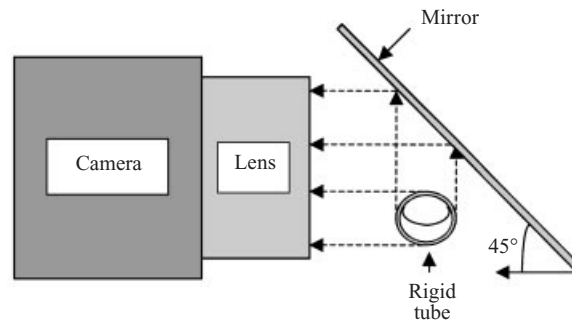
FIGURE 2. Experimental apparatus.

FIGURE 3. Dual-view visualisation depiction.

post-experimental analysis. Steady laminar flow through the test section is provided through a fixed pressure head flow system identical to that in Cavanagh & Eckmann (1999). This gravity-driven flow is represented by Q_g.

Surfactants are infused at a flow rate Q_s into the bulk flow with a system of two computer-controlled syringe pumps (Harvard Apparatus, Model 22). As shown in figure 2, the syringe pumps are integrated into the system between the temperature bath and the entrance to the test section. Therefore, when a syringe pump is activated, the total bulk flow in the test section is $Q_b = Q_g + Q_s$. A custom Y-shaped tubing connector with a modified triple lumen catheter is used to allow for the mixing of the syringe pump outputs and the bulk flow. The point of entry of the infusions is set approximately 1.8 m from the middle of the test section in order to allow for adequate mixing of the two flows. Synchronized automated on/off switching of the pumps is controlled through the LabVIEW data acquisition system.

	Acrylic tube
Tube inner diameter (cm)	0.635
Surface tension of tap H_2O, σ (dyn cm^{-1}) ($n = 15$)	63.1 ± 3.6
Bulk viscosity, μ (cP)†	0.94
Bulk density, ρ (g cm^{-3})†	0.99

† Taken from *Am. Soc. Engng Manual* **25**, 1942.

TABLE 1. Material properties at room temperature ($23 \pm 1\,^{\circ}$C).

Two syringe pumps are required in order to permit the infusion of bulk fluid in addition to various surfactant solutions. The reasoning behind the need for two pumps is straightforward. At the beginning of an experiment with the syringe pumps off ($Q_s = 0$), a bubble is held stationary at a minimum bulk flow $Q_{b,min}$ which equals Q_g. Next, the bulk fluid syringe pump is activated at Q_s which increases the bulk flow to $Q_b = Q_{b,min} + Q_s = Q_g + Q_s$. Since Q_b is now greater than the desired minimum flow rate, Q_g is manually decreased by Q_s which results in $Q_b = Q_{b,min}$. Now, when the syringe pumps are toggled such that the surfactant solution is infused instead of the bulk fluid, Q_b remains fixed at $Q_{b,min}$. Used this way, the system is designed to initiate the surfactant infusion without changing total flow in the apparatus.

Another modification of the flow system is the addition of a waste tank to collect the surfactant-containing bulk flow which has flowed through the test section. As shown in figure 2, a three-way stopcock is put in the flow line downstream from the electromagnetic flowmeter (Carolina Medical). During the surfactant experiments, this stopcock allows for the redirection of the surfactant containing bulk fluid into the waste tank, thus preventing it from being recirculated back up into the elevated reservoir containing the bulk fluid.

For these experiments, the surfactant used is sodium dodecyl sulphate (SDS) (Sigma Chemical Company) which is a highly water-soluble anionic surfactant. Although there has been considerable investigation into the effects of the hydrolysis product dodecanol on the surface activity of SDS, we have chosen to use SDS as our surfactant owing to its wide use as a model surfactant in various venues of surface and colloid research (Vollhardt & Emrich 2000). Furthermore, this surfactant is chosen because of its well-known physicochemical characteristics and because of its frequent use in previous investigations such as Zhang & Basaran (1995, 1997), Fdhila & Duineveld (1996) and Eckmann et al. (2001).

Owing to the large volume of tap water used as the bulk fluid, the system is acknowledged as being contaminated with respect to pure water. In order to examine the potential effects of the contaminants on surfactant sorption mechanics, a sample of tap water was placed in a Langmuir balance (KSV Minitrough). As the surface was compressed, no change in surface pressure was recorded indicating that the contaminants are not surface active. Additionally, representative experiments were repeated in triplicate with ultrapure water (Millipore) and when compared to the results of tap water experiments, little or no difference was discovered (see §3.2). For reference, selected experimental material properties are presented in table 1 while properties of the SDS solutions are presented in table 2. Estimates of the bulk concentration dependent adsorption and desorption rate constants are taken from Chang & Franses (1995). Note that the surface tension and contact angle values in table 2 are for SDS dissolved in ultrapure water. The values in tap water are expected to be slightly lower

CMC (mM)	8.0†
Surface tension, γ (dyn cm^{-1})	
100% CMC	37.2 ± 0.4†
10% CMC	64.5 ± 0.6†
0% CMC	68.7 ± 0.8†
Adsorption rate constant, α (cm s^{-1})	
100% CMC	3.0‡
10% CMC	5×10^{-4}‡
Desorption rate constant, β (s^{-1})	
100% CMC	2.73×10^{6}‡
10% CMC	450‡
Approximate static contact angle, Φ (deg.)	
100% CMC	28†
10% CMC	63†
Diffusivity coefficient in bulk fluid, D_b (cm^2 s^{-1})	1.76×10^{-6}§

† In Ultrapure water.
‡ Taken from Chang & Franses (1995).
§ Taken from K. J. Mysels (1986).

TABLE 2. Properties of SDS solutions.

Effective bubble size, λ	$0.8 \leqslant \lambda \leqslant 1.5$
Reynolds number, Re	$25 < Re < 530$
Capillary number, Ca	$6.14 \times 10^{-5} < Ca < 0.002$
Weber number, We	$0.0015 < We < 1.06$
Froude number, Fr_ω	$0.03 < Fr_\omega < 1.02$
Bond number, G	$0.06 < G < 0.11$
Bulk Péclet number, Pe_b	$1.5 \times 10^5 < Pe_b < 2.85 \times 10^6$
Surface Péclet number, Pe_s	$3 \times 10^5 < Pe_s < 5 \times 10^6$
Dimensionless concentration, k	$0.088 < k < 0.88$
Biot number, Bi	$40 < Bi < 4 \times 10^6$
Viscosity ratio, η	0.019

TABLE 3. Dimensionless parameter ranges.

since γ_{tap} is about 5% less than γ_{pure}, as shown in tables 1 and 2. Finally, in table 3, we present dimensionless parameter ranges derived from experimental conditions in this investigation.

2.2. *Experimental procedure*

With the system activated and calibrated, one syringe pump is loaded with two 60 cm^3 plastic syringes filled with bulk fluid while the other pump is loaded with syringes filled with a surfactant solution. Next, the infusion lines from the syringes to the Y-shaped tubing connector are flushed to remove all air. With the infusion components primed and set, the individual experiments are initiated.

Before bubble injection, the flow valves are fully opened in order to flush the system of all air bubbles. Next, the three-way stopcock is turned so that the fluid exiting from the test section is directed into the waste tank. The flow valves are then closed completely in order to have a zero bulk flow rate. With zero flow, the desired volume of air is injected into the test section, as previously described in Cavanagh

& Eckmann (1999). The bubble is positioned in the middle of the test section and allowed to stabilize for several minutes, after which the corresponding bulk flow rate and pressure difference are recorded. The bubble is held stationary under minimum bulk flow conditions. The recorded minimum bulk flow rate, $Q_{b,min}$, is used in order to determine the appropriate syringe infusion flow rate, Q_s, which is defined as

$$Q_s = \frac{C Q_{b,min}}{C_s}, \tag{2}$$

where C is the target bulk surfactant concentration and C_s is the concentration of surfactant in the syringes. The calculated value of Q_s is then programmed into the syringe pumps.

With the pumps programmed, the bulk fluid syringe pump is activated through the computer-controlled system. Since this syringe pump flow will increase the overall bulk flow of the system, the manual flow valves are adjusted to reduce the total bulk flow back to $Q_{b,min}$ as described earlier. The bubble is then allowed to restabilize for approximately 1 min, after which the syringe pumps are toggled simultaneously so that the surfactant pump is activated and the bulk fluid pump is deactivated. This toggling of the pumps, which activates the data acquisition, is computer controlled and indicated by LEDs located in the video background. During the data acquisition, both the flow rate, Q_b, from the electromagnetic flowmeter and the pressure difference, ΔP, from the differential pressure transducer are recorded. Additionally, the entire experiment is recorded to videotape.

The infusion of surfactant is continued until one of three conditions are met: (i) the bubble has been dislodged and travelled out of the test section; (ii) there is no visible long-term effect after an initial effect; or (iii) the surfactant syringes are empty. If the bubble begins to move axially within the test section, the X, Y-table is activated to keep the bubble in camera view.

Following each experiment, the system is flushed for 2–3 min at a bulk flow rate of approximately $1 \, \mathrm{l \, min^{-1}}$ in order to remove any residual surfactant in the test system. New tubes were substituted following every few experiments. The adequacy of this cleaning process is verified through the repeatability of representative experiments, as will be demonstrated in §3. The resulting output from the flushing is collected and discarded. Finally, the three-way stopcock is returned to the recirculating position and the bulk fluid is replenished. Each combination of inclination angle, bubble size, and bulk surfactant concentration is carried out either two or three times ($\omega = 65°$).

2.3. *Image analysis*

A video frame grabber board (Integral Technologies, Flashpoint 3D Lite) and a video marker/measurement system (Boeckeler, model VIA-170) are used to analyse the bubble images recorded on video for each experiment. The frame grabber board is used to acquire digital images, and the video marker/measurement system allows the user to make discrete measurements of bubble dimensions. Specifically, the Boeckeler system is used to record positional changes in upstream and downstream contact fronts as a function of time from surfactant infusion using the single-frame advancement feature of the video cassette recorder. The independent measurement of the position of the two bubble fronts allows for the analysis of the time-dependent change in the dewetted axial length.

3. Results and discussion

3.1. *Analysis of surfactant transport regimes*

Critical to the evaluation of the current experimental results is a determination of the regimes of surfactant transport in the experiments. As indicated in table 3, both Pe_b and Pe_s are of the order of 10^5 or larger, indicating that, both in the bulk and on the interface, convective transport of surfactant dominates. With this result, we may assume that diffusion is negligible in regions where the fluid velocity is of $O(U_b)$ or larger. Stebe *et al.* (1991) and Wang *et al.* (1999) observed that, if surfactant desorption from the interface is fast relative to surface convection ($Bi \gg 1$) and if the bulk concentration is elevated ($k > 1$), surface remobilization is likely to occur. This is attributable to the elimination of the desorptive and diffusive barriers to surfactant exchange between the surface and the bulk, as explained in Stebe *et al.* (1991).

For the current investigation, we have used bulk concentration dependent adsorption and desorption rate constants from Chang & Franses (1995) in order to evaluate Bi and k. Bi is determined to be in the range $40 < Bi < 4 \times 10^6$, indicating that the desorption kinetics are indeed fast when compared to the surface convection. The dimensionless bulk concentration parameter, k, is determined to be in the range $0.088 < k < 0.88$, indicating either low or nearly order one concentrations. The values of these parameters for our investigation indicate that remobilization may occur, especially for experiments in which Bi and k are near their maxima.

Furthermore, as $Pe_b \gg 1$, the bulk surfactant concentration gradients oriented normal to the bubble surface will be confined to the small boundary layer near the surface (Stebe *et al.* 1991). With these gradients being large, diffusion to the interface is predicted to be rapid and therefore the surfactant transport in this investigation is not expected to be diffusion limited in regions of the interface where velocities are of $O(U_b)$ or larger. Should portions of the bubble interface experience significantly reduced velocities owing to recirculation zones or flow separation, diffusion from the bulk and along those portions of the interface may become significant. Overall, the surfactant transport in this investigation is likely to follow mixed kinetic (or adsorption limited) behaviour. This regime of behaviour is opposite to the insoluble limit behaviour described by Wang *et al.* (1999).

3.2. *Overall bubble response to surfactants*

In the current experiments, we have analysed the effects of an infused soluble surfactant on stationary bubbles of various sizes in tubes at various inclination angles. For the 24 parameter combinations of interest, we have observed six dynamic responses of the bubbles. These responses are dependent upon bubble size, tube inclination, and bulk surfactant concentration. For all bubble images presented, the upper portion is the reflected top view of the tube with the top edge of the upper image corresponding to the front of the actual tube (see figure 3). The flow direction is from left (upstream) to right (downstream). Note that all bubbles in these experiments are held stationary at the lowest flow rate possible, i.e. at Re_{min} (see Cavanagh & Eckmann 1999 for details).

In figure 4, we present the bubble responses in plots of Fr_ω vs. λ for $C = 100\%$ CMC and $C = 10\%$ CMC, where CMC denotes critical micelle concentration. The symbols correspond to the type of bubble behaviour observed in response to the surfactant. We have also included the results of separate trials of experiments conducted individually with new tubes and with ultrapure water. Results of these experiments are identified with + markers located next to the symbols. For $C = 100\%$ CMC, $\lambda = 1.5$, and
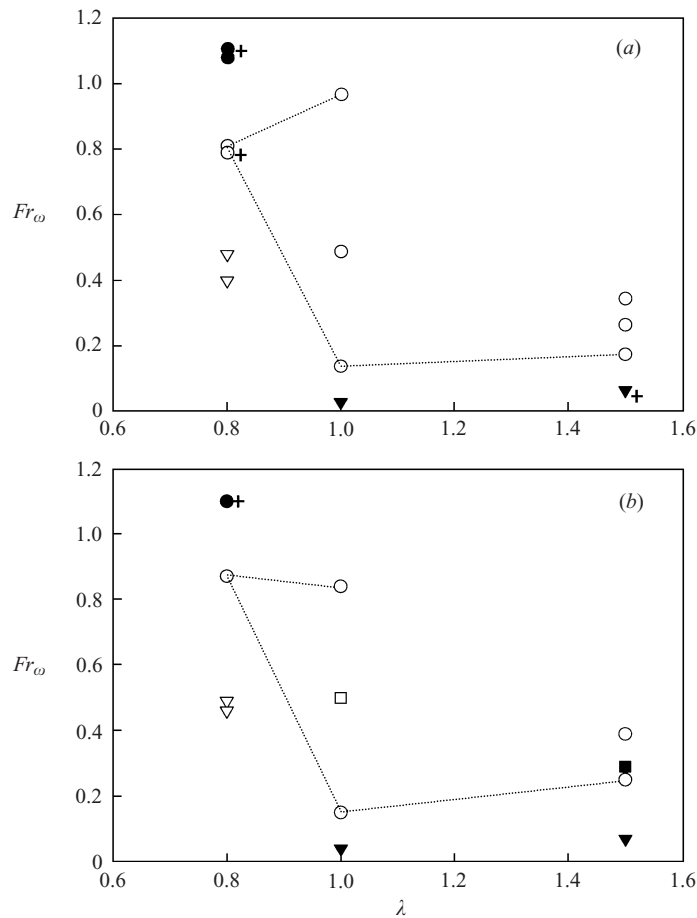
FIGURE 4. Fr_α *vs.* λ for (*a*) $C = 100\%$ CMC and (*b*) $C = 10\%$ CMC. ●, interfacial deformation; ○, detachment and upstream translation; ▼, non-dewetted upstream translation; ▽, non-dewetted downstream translation; ■, dewetted upstream translation; □, pulsatile upstream translation.

$Fr_\omega = 0.07$ and for $C = 10\%$ CMC, $\lambda = 0.8$, and $Fr_\omega = 1.1$ the tap water and ultrapure water results directly overlap in figure 4. As the results of these representative experiments closely match the tap water results, we conclude that there are minimal effects on bubble response resulting from using tap water, our cleaning process and our frequency of tube replacement.

For $C = 100\%$ CMC (figure 4*a*), a central region of bubble behaviour is graphically surrounded by three regions of different behaviours. The central region contains a majority of the experimental combinations examined and it is in these experiments that we observed the stationary dewetted bubbles detach from the tube wall and rise upstream against the flow. Before and after surfactant images, displaying this detachment and upstream translation behaviour, are presented in figures 5(*a*) and 5(*d*) for $\lambda = 0.8$ at $\omega = 25°$ and $\lambda = 1.0$ at $\omega = 45°$, respectively. In both sets of images, note the lack of an air–tube interface in the second image in addition to the enhanced protrusion of the bubble into the flow field. These surfactant-laden bubbles are rising upstream. Also in figure 4, we observe that for $\lambda \geqslant 1.0$, all bubbles (dewetted and non-dewetted) are observed to move upstream in response to the
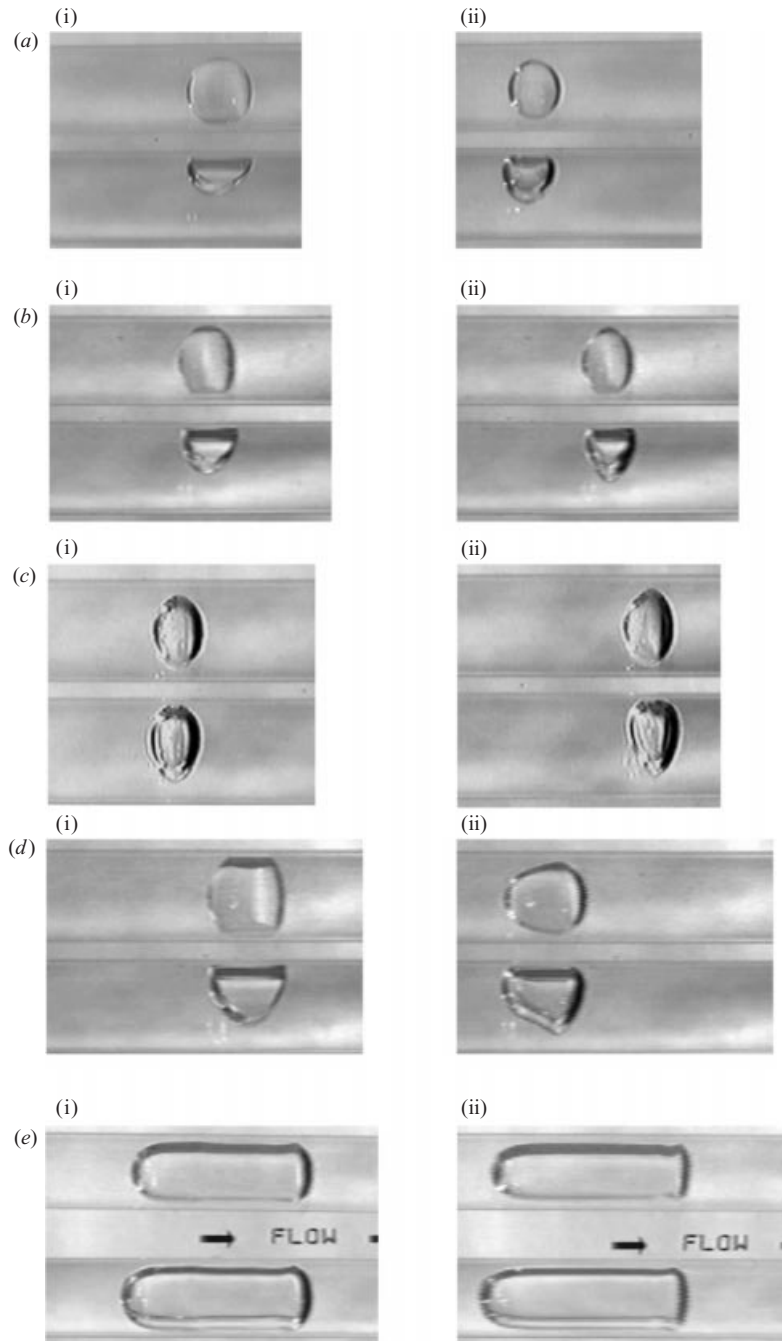
FIGURE 5. (i) Before and (ii) after surfactant bubble images for $C = 100\%$ CMC. (*a*) $\omega = 25°$, $\lambda = 0.8$; (*b*) $\omega = 45°$, $\lambda = 0.8$; (*c*) $\omega = 65°$, $\lambda = 0.8$; (*d*) $\omega = 45°$, $\lambda = 1.0$; (*e*) $\omega = 90°$, $\lambda = 1.5$.

surfactant, indicating that bubble size is important in predicting bubble response to surfactant infusion. Assuming that the buoyancy force remains constant, the surfactant is probably modifying the viscous drag, pressure drag and/or contact forces, as discussed next.

In all of the experiments in this central region, we observe a general process by which the bubble detaches. First, as the surfactant adsorbs to the interface, the bubble begins to bulge upstream and become more streamlined in the flow field. Next, the downstream edge of the contact perimeter begins to move upstream while the upstream end of the contact perimeter remains fixed or moves slowly. Owing to the bulging and the downstream-moving contact edge, the dewetted area begins to shrink while the air–water interfacial area dilates. Although this dilation of the air–water interface would tend to redistribute the surfactant on the interface, the high concentration of surfactant in the bulk permits rapid resaturation of the interface, as indicated by elevated adsorption rate constants in Chang & Franses (1995). This description of the general detachment process highlights the two sequential phenomena involved in producing detachment, i.e. the initial shape change of the bubble followed by the movement of the contact lines.

A general mechanism is put forth to describe the complex dynamic process by which bubbles detach. As the surfactant-containing bulk fluid reaches the bubble interface, surfactant will adsorb to the interface and be convected to the downstream end of the bubble where it will lower the local surface tension. Owing to the high rate of desorption relative to surface convection ($Bi > 1$), the surfactant is not likely to accumulate in this region and the bubble may attain uniform surface distribution of surfactant, thereby keeping the interface mobile. Since no Marangoni stresses will develop, the viscous drag term in (1) will remain negligible. The entire bubble interface, however, will have a lower surface tension which will alter the normal forces on the surface, as governed by Laplace's equation. This force modification will probably act in conjunction with the local fluid flow and contact mechanics to produce an increase in local interfacial curvature, especially at the downstream end (figure 5$b$ii, $d$ii). This contraction of the air–water interface will decrease A_z, which would lead to a reduction of the pressure drag force. With this force reduced, the buoyancy force will dominate, resulting in the observed upstream bulge that occurs rapidly in response to the surfactant adsorption owing to the rapid surface convection over a majority of the bubble.

Following this initial bulge, the surfactant on the interface will diffuse to the dewetted perimeter where it will alter the contact mechanics. As observed, this second effect is expected to lag the first as $Pe_s \gg 1$ and the local bulk fluid velocities in the vicinity of the dewetted perimeter are likely to be small compared to U_b owing to the no-slip of the bulk fluid on the tube wall. The local fluid mechanics in the vicinity of the dewetted perimeter will be dependent upon the shape of the bubble, λ, ω and Re. As was shown in Cavanagh & Eckmann (1999), air bubbles in acrylic tubes may be held stationary over a range of Re owing to contact angle hysteresis. In order for a bubble to move axially while remaining dewetted to the tube wall, critical advancing and receding contact angles must be overcome. When dealing with liquid drops on solid surfaces, the contact angle is commonly defined as the angle within the liquid phase from the solid substrate to the gas–liquid interface. In the current experiments, the advancing and receding contact angles are at the downstream and upstream edges of the bubble, respectively (see figure 1). As noted earlier, Eckmann *et al.* (2001) have demonstrated that the presence of SDS in water drops on acrylic surfaces decreases both the advancing and receding contact angles. Therefore, the presence of the surfactant in the current experiments will probably aid in the advancement of the downstream edge of the bubble while it concurrently impedes the advancement of the upstream edge. This effect, when combined with the buoyancy-driven bulging, leads

to bubble detachment. Once the bubble has detached, contact forces are no longer involved and bubble motion is governed by the interaction of the drag and buoyancy forces.

For $Fr_\omega < 0.1$ in figure 4(a), indicating that the gravitational forces are approximately 10 times greater than the inertial forces, bubbles of $\lambda = 1.0$ are observed to rise upstream in response to the SDS infusion. In contrast, bubbles of $\lambda = 1.5$ are observed to translate downstream initially at a fixed velocity in response to surfactant delivery and then rapidly switch direction and accelerate up the tube against the bulk flow. As these two bubbles are held stationary at approximately the same Re in agreement with Cavanagh & Eckmann (1999), the primary difference between the experiments is bubble size.

For the three trials of the $\lambda = 1.5$ experiment, the period of downstream translation was determined to be 20.7 ± 3.8 s after which the bubble changed direction and rose upstream.

Images for $\lambda = 1.5$ are presented in figure 5(e). As these bubbles are in tubes at $\omega = 90°$, no drying has occurred and contact forces are not involved. As the surfactant is convected to the rear of the bubble and Marangoni stresses develop, a small region of increased local curvature is observed at the downstream edge, similar to that described in Stebe *et al.* (1991). This curvature modification is probably due to the alteration of the surface tension forces on the interface in addition to the local fluid mechanics. Also, with respect to the before surfactant image (figure 5ei), the cylindrical portion of the post-surfactant rising bubble (figure 5eii) possesses a much smoother surface, as would be expected since the Marangoni stresses would tend to oppose any deformation, as suggested by Yon & Pozrikidis (1999). Finally, note that owing to the surfactant, the diameter of the bubble has decreased slightly, indicating a decrease in the radial cross-sectional area, A_z, of the bubble. This decrease in diameter is accompanied by an observed increase in bubble length.

One potential explanation for this observed bi-directional response of the $\lambda = 1.5$ bubbles at $\omega = 90°$ is the concept of surface remobilization discussed earlier. Initially, when the surfactant adsorbs to the interface, it is convected along the surface to the rear of the bubble, thereby establishing the Marangoni stresses that retard the surface velocity and increase the drag on the bubble. Therefore, under fixed flow rate conditions, the increased viscous drag on the bubble will produce movement in the downstream direction, as observed. The surfactant accumulation on the downstream edge of the bubble may also produce a remobilized interfacial region similar to that described by Stebe & Maldarelli (1994). This remobilized region would tend to reduce the drag on the bubble as the interfacial mobility in that region has been restored owing to the elimination of surface tension gradients. Surfactant would not be expected to diffuse from the remobilized region toward the upstream end of the bubble since $Pe_s \sim 8 \times 10^5$. As more SDS adsorbs to the bubble interface from the bulk fluid, a larger percentage of the bubble would be included in the remobilized region, which would tend to decrease the drag on the bubble. However, as the remobilized region advances toward the upstream bubble end, the Marangoni stresses in the non-remobilized region would increase owing to the increase in the surface tension gradient. Eventually, the entire bubble would become remobilized, the Marangoni stresses would be eliminated and the bubble would tend to return to the initial stationary state. In the experiments, however, we observe the bubble to translate upstream indicating that another component of the force balance has been altered. This component is the pressure drag force that is probably reduced owing to the slight reduction in the cross-sectional area of the bubble. This reduction allows

the buoyancy force to dominate resulting in upstream translation of the remobilized bubble.

For $\lambda = 0.8$ and $Fr_\omega < 0.5$, the surfactants cause a shape change in the bubble and induce downstream motion of the initially non-dewetted bubbles. Although $Fr_\omega < 1$ for these experimental conditions indicating that the gravitational forces are greater than the inertial forces, the bubble response is to move in the direction of the bulk flow. This downstream movement is most probably a result of the increased drag force that arises from the development of Marangoni stresses on the bubble interface which would act in a direction opposite to that of the flow. As these two experiments are in tubes at $\omega = 65°$ and $90°$, the bubbles never dry the tube wall and, hence, no contact forces are involved. Images for $\lambda = 0.8$, $\omega = 65$, with $C = 100\%$ CMC are presented in figure 5(c). Note the increased curvature in the equatorial-like region which is most probably a result of modified surface tension forces and the local fluid flow at this point. As the bubbles for these experiments passed out of the field of view of the camera in a relatively short time, we are currently unable to investigate the possible remobilization of these bubbles. Given that $Bi > 3 \times 10^5$ for these experiments, remobilization is likely to occur.

For $\lambda = 0.8$ and $Fr_\omega \sim 1$, we observe that the bubbles experience only geometric shape changes without any axial translation (figure 5b). These dewetted bubbles decrease in axial length and protrude further into the flow in response to the infused surfactants. As indicated in Cavanagh & Eckmann (1999), bubbles of this size in tubes at $\omega = 45°$ dry the tube wall and require higher bulk fluid velocities to maintain a stationary axial position. In the current experiment, neither the buoyancy force nor the drag force acting on the bubble is sufficient to overcome the contact forces that retard bubble motion. Additionally, owing to the high fluid velocity in this experiment relative to the other experiments, flow separation may occur somewhere on the downstream side of the bubble. This separation would tend to convect surfactant away from the bubble, thereby preventing SDS from reaching the downstream contact edge and reducing the critical advancing contact angle required for motion. As $Pe_s \sim 8 \times 10^5$, surfactant would not be expected to diffuse to the downstream contact edge. Although no previous investigations have analysed the possible flow separation in a bulk fluid passing a three-dimensional dewetted gas bubble in an inclined cylindrical tube, Feng & Basaran (1994) and Durbin (1988) do provide some evidence that this is likely to be occurring in the current experiments.

When C is decreased to 10% CMC, two experimental parameter combinations reveal new behaviours, whereas the remainder display the same overall bubble response as that observed at the higher C. The responses of the bubbles at this lower bulk surfactant concentration are presented in figure 4(b). Both new responses occur in tubes inclined at $\omega = 45°$. For $\lambda = 1.5$ and $Fr_\omega = 0.29$ (solid square), the initially dewetted bubble (figure 6ai) never detaches from the tube wall as it moves upstream (figure 6$a$ii) in response to the surfactant. In this experiment, we observe that the bubble bulges upstream as the surfactant adsorbs to the interface and is convected to the rear of the bubble. The downstream contact edge does move upstream; however, it never catches up to the upstream edge, as would be required for detachment. Since the bulk surfactant concentration has been decreased, less surfactant reaches the downstream contact edge. Without a sufficient surface concentration of surfactant being achieved, the net reduction of the advancing contact angle is lessened and therefore the velocity of this edge is decreased. Furthermore, the upstream contact edge would be less likely to remain pinned to the wall since less SDS has made its way to the upstream contact edge.
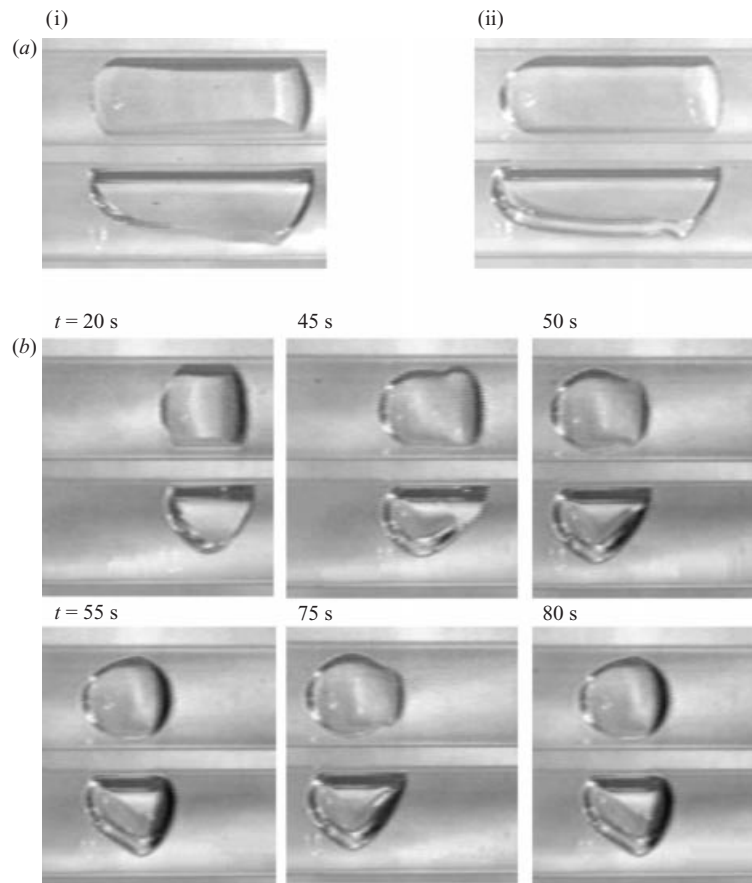
(i)   (ii)

(a)

t = 20 s   45 s   50 s

(b)

t = 55 s   75 s   80 s

FIGURE 6. (a) Bubble images with $C = 10\%$ CMC. (i) Before and (ii) after images for
$\omega = 45°$, $\lambda = 1.5$. (b) Sequence of images for $\omega = 45°$, $\lambda = 1.0$.

For $\lambda = 1.0$ at $Fr_\omega \sim 0.2$ ($\omega = 45°$), a very dynamic response is revealed. In this experiment, the initially dewetted bubble is found to begin repeatedly to move upstream and nearly detach, yet complete detachment is not achieved as it attains a new quasi-steady state. A series of images from one of these experiments is presented in figure 6(b). The first image is that of the bubble before the surfactant has arrived ($t = 20$ s). As the surfactant adsorbs to the interface, the bubble begins to bulge upstream ($t = 45$ s) and the downstream edge of the contact perimeter begins to move upstream ($t = 50$ s). While the contact perimeter is shrinking, the gas–liquid interface is dilating, thereby redistributing the surfactant on the interface. Owing to the low bulk surfactant concentration, the surfactant may not adsorb to the interface fast enough, allowing the development of Marangoni stresses on the interface which oppose the upstream bulging resulting in a new quasi-steady state ($t = 55$ s). As time progresses, more surfactant adsorbs to the interface which may increase the mobility of the interface and again initiate the upstream bulging ($t = 75$ s). Again, as the interface dilates, the surfactant may be redistributed, thereby inducing Marangoni stresses which result in the bubble reaching a new quasi-steady state. This behaviour of the bubble continues until the experiment is concluded. Furthermore, since $Bi > 1$, the surfactant would be expected to desorb from the interface, thereby

preventing the complete saturation of the interface with surfactant. This would allow the pulsatile response to be sustained. Without knowing the fluid mechanics in the vicinity of the bubble and the time-dependent distribution of surfactant on the air–water interface, we can only speculate as to the phenomena underlying this pulsatile response.

Another effect of decreasing C is observed for $\lambda = 1.5$ and $\omega = 90°$ where the period of downstream translation is less than that observed for the higher C mentioned earlier. For low C, the period of translation is 9.7 ± 5 s which is shorter than that observed for high C which is 20.7 ± 3.8 s. This result is expected since the high C experiment should produce larger initial Marangoni stresses on the interface, thereby producing higher drag on the bubble. This increased drag should result in a longer downstream translation time.

3.3. *Pressure difference modifications*

In addition to analysing the geometric response of the bubbles to the infused surfactant, we also investigate the response of the driving pressure within the test section. Note that for all of the experiments, the bubbles are held stationary at Re_{min} and it is expected that the flow rates remain constant throughout each experiment.

In the previous section, we described that for $\lambda = 0.8$ at $\omega = 45°$ and $C = 100\%$ CMC, the bubble displayed only a shape change and when C was decreased to 10% CMC, the same response was observed. Although the image analysis indicates that these two experiments are similar, the pressure waveforms, presented in figure 7, do provide an indication of their difference. In figure 7, flow rates are scaled as Re. Measured pressure differences, ΔP, are scaled against the theoretical Poiseuille flow pressure, ΔP_p, for the constant flow rate in the tube, i.e. $\Delta P^* = \Delta P / \Delta P_p$. In the high (figure 7a) and low (figure 7b) C experiments, Re is equal to approximately 525 and 515, respectively, showing that the flows are similar in nature. Although we observe the overall increases in ΔP^* to be similar ($\sim 15\%$), the increase in pressure when $C = 100\%$ CMC occurs much more rapidly than at the low C. The higher bulk surfactant concentration leads to a faster adsorption of SDS to the interface, as indicated by increasing adsorption rate constants for increasing bulk SDS concentrations in Chang & Franses (1995). The faster adsorption permits rapid saturation of the interface with the SDS molecules thereby accelerating the development of the shape modifications. To demonstrate that similar results were observed for the remaining two trials of these parameter combinations, we have included in figure 7(c) combined Re and ΔP^* waveforms for all three replicates of $\lambda = 0.8$ at $\omega = 45°$ and $C = 10\%$ CMC. The overlapping of these results verifies the repeatability of the experimental apparatus.

Bubbles that detach from the tube wall and rise in the upstream direction show a significant increase in ΔP^*, as shown in figure 8 for $\lambda = 0.8$, $\omega = 25°$ and both levels of C. In these two experiments, no significant difference is found in the rate at which the surfactant induces the upstream rise and detachment. Analysis of the corresponding video images also reveals no distinctions between the two experiments as both bubbles behave similarly. This behaviour, similar in the two experiments, may be attributed to the small air–water interfacial area over which the surfactant acts. Owing to the small interfacial area, the different adsorption rate constants for the different C values have little effect in inducing the upstream bulge and detachment. Both adsorption rates are sufficient to induce this immediate response. The difference in the times at which the effects of the surfactant are observed in the pressure
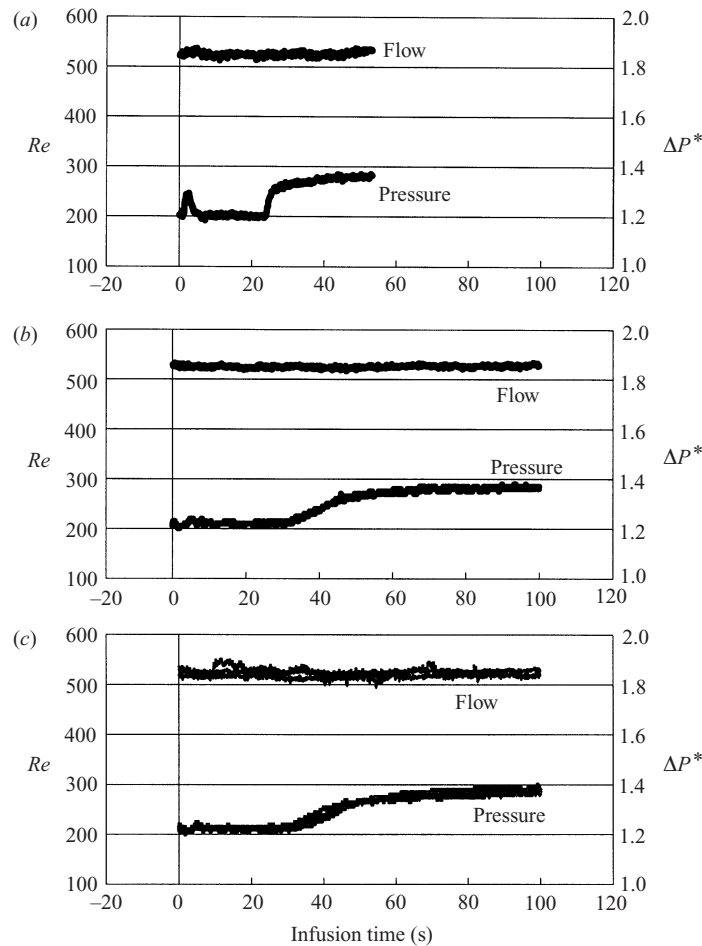
FIGURE 7. *Re* and ΔP^* *vs.* infusion time for $\omega = 45°$, $\lambda = 0.8$. (*a*) $C = 100\%$ CMC. (*b*) $C = 10\%$ CMC. (*c*) Combined results of three replicates of (*b*).

difference waveforms is explained by the fact that the bubbles were held stationary at different axial locations in the tube.

As a further example of the effects of SDS on the pressure difference waveform, we examine the case of $\lambda = 1.0$, $\omega = 45°$ for both C levels. For $C = 100\%$ CMC, images of the bubble detaching from the tube and rising were shown in figure 5(*d*). The corresponding waveforms are presented in figure 9(*a*). In this experiment, we observe that the bubble bulges upstream, detaches from the wall and translates in the upstream direction. In the pressure waveform, we observe a slight drop in ΔP^* at $t \sim 40$ s corresponding to the brief streamlining of the bubble as it bulges, followed by a sharp increase in the pressure owing to the upstream rise of the bubble. As described in the previous section, when C is decreased to 10% CMC, the bubble displays a pulsatile response to the surfactant (figure 6*b*). The corresponding pressure waveform (figure 9*b*) reveals an initial decrease in pressure ($t \sim 50$ s) followed by a sharp increase in ΔP^*. This increase is only temporary as, at $t \sim 75$ s, we again observe a drop in ΔP^* as the bubble bulges upstream and streamlines as it attempts to detach. After the initial bulging, the bubble experiences three more detachment
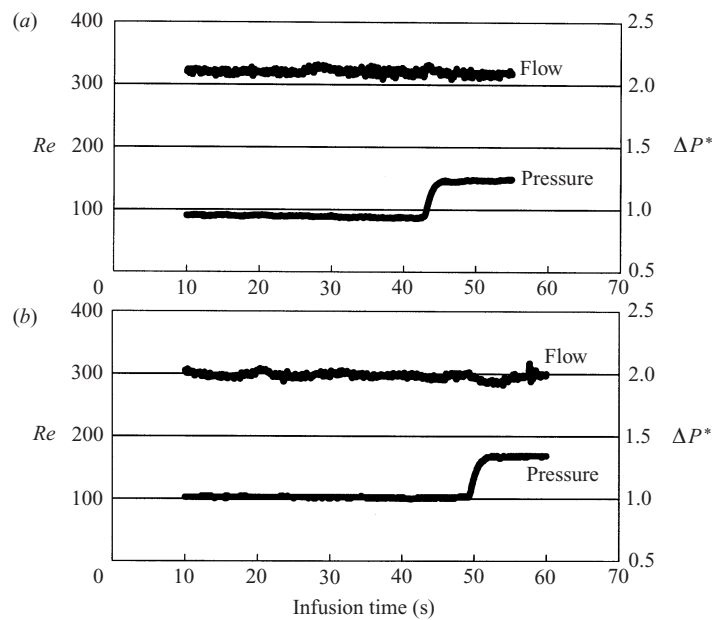
FIGURE 8. Re and ΔP^* *vs.* infusion time for $\omega = 25°$, $\lambda = 0.8$. (*a*) $C = 100\%$ CMC.
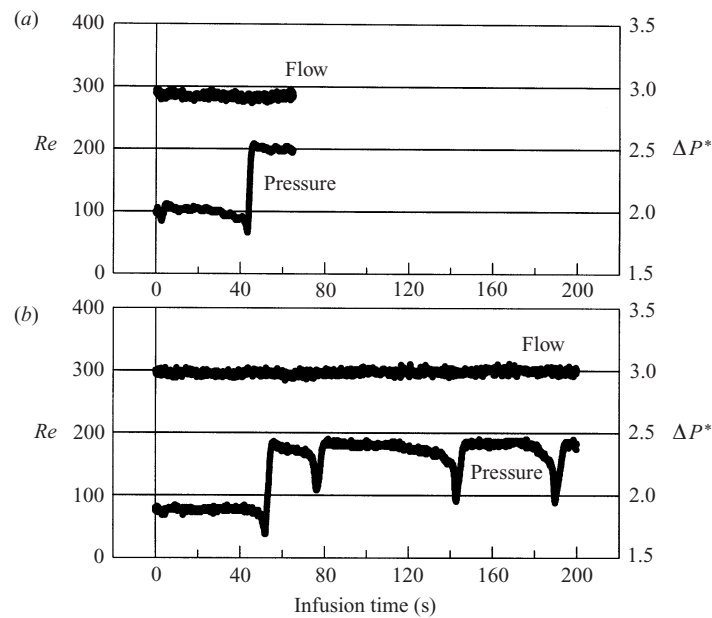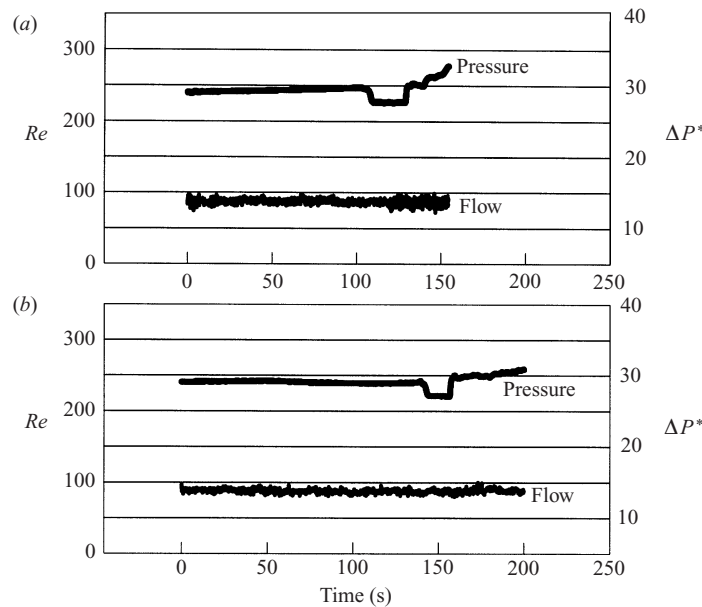(*b*) $C = 10\%$ CMC.

FIGURE 9. Re and ΔP^* *vs.* infusion time for $\omega = 45°$, $\lambda = 1.0$. (*a*) $C = 100\%$ CMC.
(*b*) $C = 10\%$ CMC.

attempts, none of which lead to complete detachment from the tube wall. Similar behaviour is observed in the remaining two replicates of this experiment.

As a final example of the effects of SDS on the pressure gradients, we present the pressure and flow waveforms for both C levels with $\omega = 90°$ and $\lambda = 1.5$ (figure 10).

FIGURE 10. *Re* and ΔP^* *vs.* infusion time for $\omega = 90°$, $\lambda = 1.5$. (*a*) $C = 100\%$ CMC.
(*b*) $C = 10\%$ CMC.

In the previous section, we discussed the bi-directional movement of these bubbles. As discussed in Cavanagh & Eckmann (1999), these large bubbles in vertical tubes have a significant effect on the pressure gradient required to maintain constant flow in the tubes. When $C = 100\%$ CMC (figure 10*a*), the initial response for the bubble is downstream translation, as indicated by the sudden drop in pressure at $t \sim 110$ s. After approximately 20 s, the bubble reverses direction and the pressure gradient increases above the pre-surfactant values as the bubble accelerates upstream. A similar response is observed for the lower C experiment (figure 10*b*), except for the shortened downstream translation time, as discussed in the previous section.

In figure 11, we present an overall analysis of the modifications of ΔP^* as a function of λ for varying $\omega = 25°$, $45°$ and $65°$. Pressure modifications for $\omega = 90°$ are not included owing to the dynamic pressure responses. We have used a ratio of the final (post-surfactant) pressure difference, ΔP_f^*, to the initial (pre-surfactant) difference, ΔP_i^*, to quantify the pressure difference modifications. Note that some experiments have not been included, e.g. $\lambda = 1.5$ with $\omega = 65°$, since the pressure waveforms for these experiments were erratic in that no exact ΔP_f^* could be determined owing to the dynamic response. In figure 11, we observe that for $\omega = 25°$ (figure 11*a*), the average pressure modification decreases with increasing λ whereas for $\omega = 45°$, $65°$ (figure 11*b,c*) the opposite relation is found. Also, for all ω and λ examined, C does not appear to have a significant effect on the overall modifications of ΔP^*.

3.4. *Contact edge velocities*

As stated earlier, not only do the infused surfactants modify the air–water interface, but they also alter the contact mechanics along the line where the air, tube and water interact. A quantitative analysis of the contact mechanics will provide further insight and evidence for a mechanistic explanation of the experimental observations. This analysis is performed using the experimental video along with the video
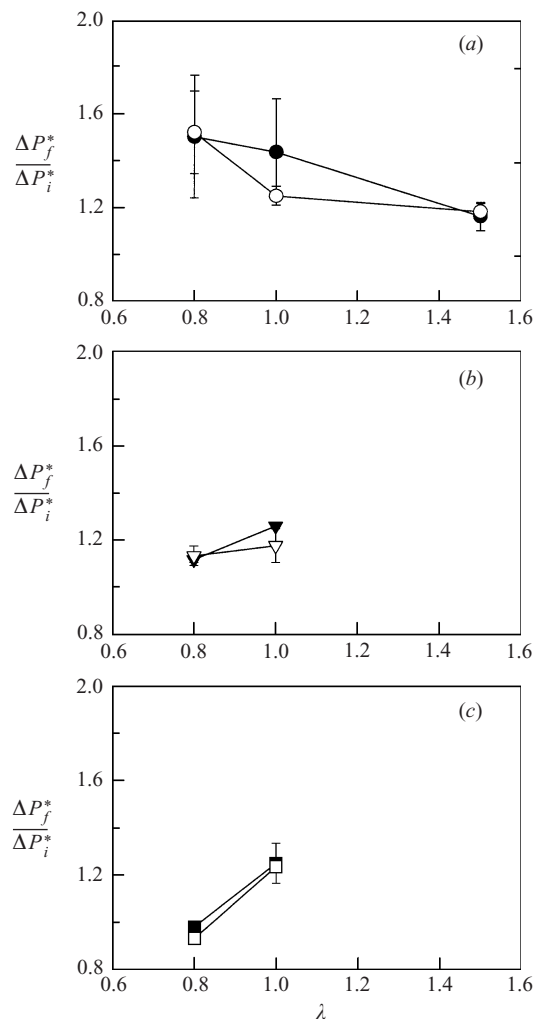
FIGURE 11. $\Delta P_f^* / \Delta P_i^*$ *vs.* λ. (*a*) ●, $\omega = 25°$ and $C = 10\%$ CMC; ○, $\omega = 25°$ and $C = 100\%$ CMC. (*b*) ▼, $\omega = 45°$ and $C = 10\%$ CMC; ▽, $\omega = 45°$ and $C = 100\%$ CMC. (*c*) ■, $\omega = 65°$ and $C = 10\%$ CMC; □, $\omega = 65°$ and $C = 100\%$ CMC.

marker/measurement system described earlier. For the experiments in which the tube wall dewets, we monitor the position of the contact edges as a function of time. With respect to the bubble images (e.g. figure 5), the contact edges are identified as the furthest upstream, z_u, and downstream, z_d, points where all three phases meet. These two points form a line segment, the dewetted length L_D (see figure 1). Monitoring the movement of these two points provides a measure of contact edge velocities similar to those found in Schleizer & Bonnecaze (1999) and also allows us to quantify the change in L_D as a function of time. Additionally, the tracking of these two points through video analysis is insensitive to both the parallax effects of tube wall curvature and the mismatch of the refractive indices.

In figure 5(*b*), we display the effects of a surfactant infusion of $C = 100\%$ CMC on a bubble of $\lambda = 0.8$ with $\omega = 45°$. In all of the trials of this experiment in addition to the corresponding trials at $C = 10\%$ CMC, we observe that the bubbles decrease in axial length and protrude further into the flow field without detaching. In figure 12,
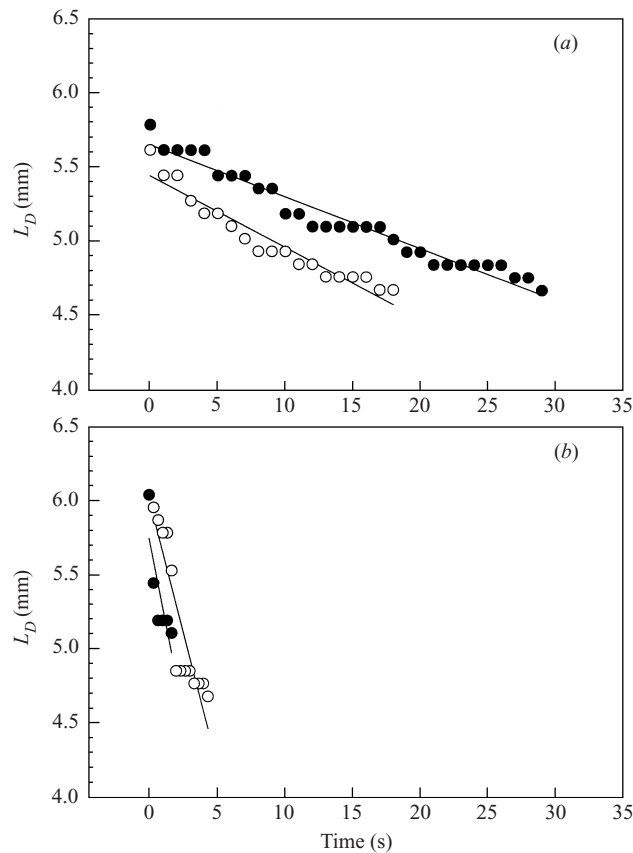
FIGURE 12. L_D *vs.* time for $\omega = 45°$, $\lambda = 0.8$. (*a*) ●, $C = 10\%$ CMC Trial 1; ○, $C = 10\%$ CMC Trial 2. (*b*) ▼, $C = 100\%$ CMC Trial 1; ▽, $C = 100\%$ CMC Trial 2. Solid lines indicate best fit lines.

we display our analysis of the behaviour of L_D as a function of time for two trials at each surfactant concentration. L_D is defined as the difference between the positions of the contact edges, i.e. $L_D = z_u - z_d$. Linear regression is used to find the slope of each line which represents the rate, dL_D/dt, at which L_D is changing. In determining the average rate, dL_D/dt^+, for each level of C, we observe a ten-fold difference in that $dL_D/dt^+ = 0.041$ mm s^{-1} for $C = 10\%$ CMC (figure 12*a*) and $dL_D/dt^+ = 0.41$ mm s^{-1} for $C = 100\%$ CMC (figure 12*b*). Although there is some variation of the velocities within each level of C, the order of magnitude difference remains constant. This result demonstrates that the high bulk surfactant concentration produces a faster moving downstream contact edge that is in agreement with the pressure gradient behaviour shown in figure 7.

We also analyse the contact edge velocities for experiments in which the bubbles detach from the wall at both levels of bulk surfactant concentration. The first experiment examined corresponds to $\lambda = 1.0$, $\omega = 25°$ and $C = 10\%$ CMC with the images from this experiment presented in figure 13. In figure 14, we present the axial positions of the contact edges along with their difference as a function of time. The time at which all three curves converge to zero is the time at which the bubble has detached from the tube wall. Data were acquired from the video by going to the point of detachment and working in reverse to a point where the
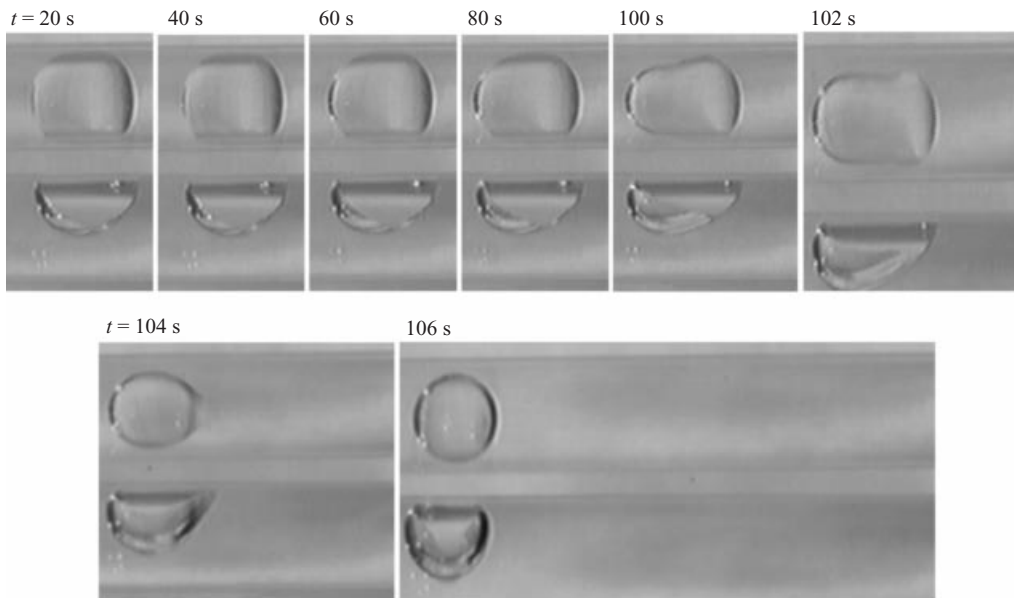
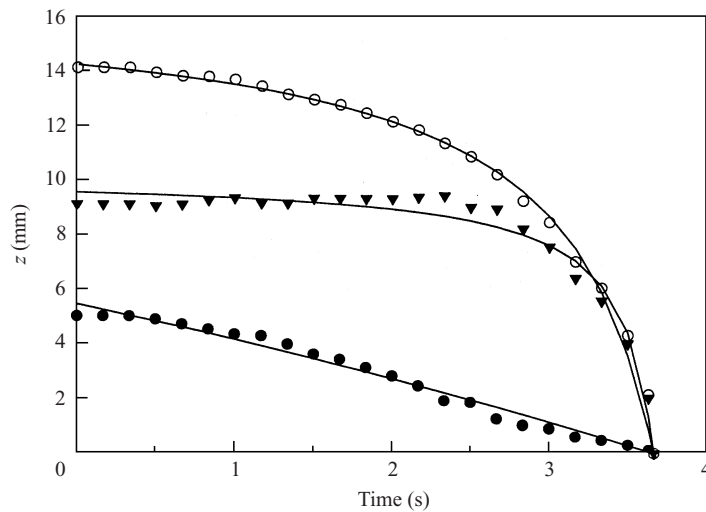FIGURE 13. Sequence of bubble images for $\omega = 25°$, $\alpha = 1.0$, and $C = 10\%$ CMC.

FIGURE 14. z *vs.* time for $\omega = 25°$, $\lambda = 1.0$ and $C = 10\%$ CMC. $\bigcirc$, downstream contact edge position z_d; $\bullet$, upstream contact edge position z_u; $\blacktriangledown$, dewetted length L_D. Solid lines indicate best-fit hyperbolas.

bubble is stable. Note that L_D is initially approximately 8.5 mm and remains near this value until $t \sim 2.5$ s. Although L_D is constant over this period, both the upstream and downstream contact edges are moving upstream as indicated by their changing positions. At $t \sim 2.5$ s, the downstream edge experiences a rapid acceleration while the upstream edge remains at a fixed velocity. This increasing velocity difference results in the dewetted length shrinking rapidly until $L_D = 0$ at $t \sim 3.7$ s, at which time the bubble has fully detached from the wall. This behaviour is similar to detachment behaviour mentioned by Schleizer & Bonnecaze (1999). Although effects of the surfactant on the contact edge velocities were observed over the entire time
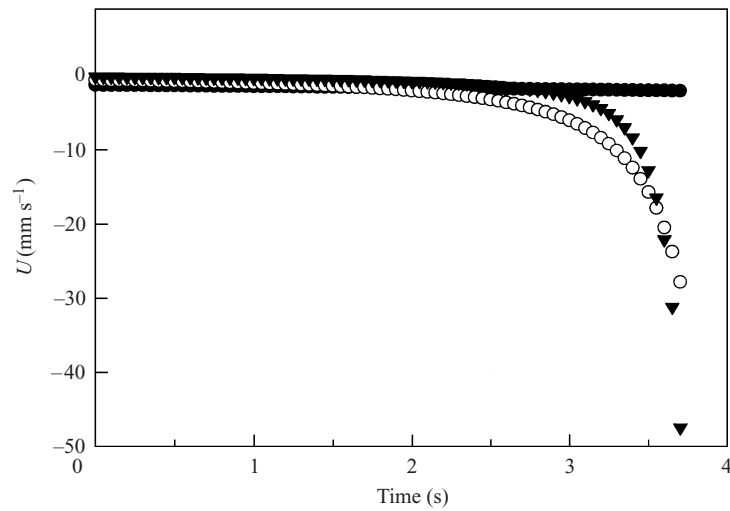
D. P. Cavanagh and D. M. Eckmann

FIGURE 15. *U vs.* time for $\omega = 25°$, $\lambda = 1.0$ and $C = 10\%$ CMC. $\bigcirc$, downstream contact edge velocity U_d; $\bullet$, upstream contact edge velocity U_u; $\blacktriangledown$, time rate of change of dewetted length, dL_D/dt.

of interest, the actual time for detachment from the tube wall, defined as the time it takes for L_D to go from a constant length to zero, is in the range of 1–1.5 s. Similar results were observed in additional trials of these experimental parameters. These times relate well to those presented by Chang & Franses (1995) whose plots of $\gamma(t)$ used the modified Langmuir–Hinshelwood adsorption model. Their predictions show decreasing surface tensions as time progresses and more surfactant adsorbs to the interface. Although they compared the model to experimental data only for short time ($t \sim 0.4$ s), their final γ values are similar to those presented in table 2 for the current experimental investigation. From this, we can conclude that the time scales of adsorption and bubble detachment are of the same order of magnitude.

The data for the position of the two contact edges, z_u and z_d, appeared hyperbolic and were fitted by a least-squares regression to the general form:

$$z_i(t) = a_i(t_{max} - t)[b_i + t_{max} - t]^{-1}, \tag{3}$$

in which t_{max} is the duration of the period of detachment and the constants a_i and b_i were determined by the fitting algorithm. In figure 14, we present the best-fit hyperbolas as solid lines overlaying the plots of z_d, z_u and L_D. Equation (3) also provides a continuous function that can easily be differentiated and evaluated using the constants obtained. Thus, we can determine the velocity of the contact edges and the rate of change of the dewetted length as a function of time. A plot of this is presented in figure 15, with negative velocities indicating upstream movement of the contact edge and resultant shrinkage of the dewetted surface area. As expected, we observe a small, nearly constant velocity, U_u, for the upstream edge of the bubble while the downstream edge velocity, U_d, is observed to be nearly constant to $t \sim 1.5$ s, after which it accelerates rapidly until detachment occurs. The downstream contact edge accelerates until its peak velocity is in the vicinity of 50 mm s^{-1} just prior to bubble detachment. The difference between these two curves provides a measure of the speed, i.e. dL_D/dt, at which the dewetted length decreases to zero.

For the same λ and ω just discussed, but with C increased to 100% CMC, we observe a similar detachment process, as shown in figure 16. Note that the initial L_D
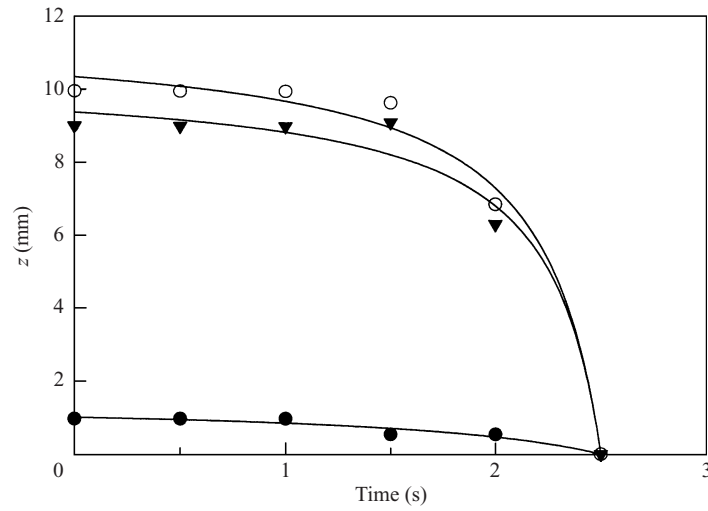
FIGURE 16. z *vs.* time for $\omega = 25°$, $\lambda = 1.0$ and $C = 100\%$ CMC. $\bigcirc$, downstream contact edge position z_d; $\bullet$, upstream contact edge position z_u; $\blacktriangledown$, dewetted length L_D. Solid lines indicate best-fit hyperbolas.
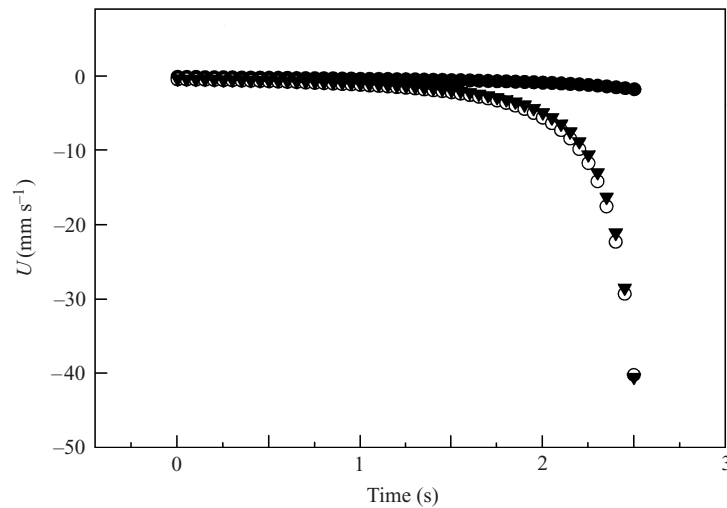

FIGURE 17. U *vs.* time for $\omega = 25°$, $\lambda = 1.0$ and $C = 100\%$ CMC. $\bigcirc$, downstream contact edge velocity U_d; $\bullet$, upstream contact edge velocity U_u; $\blacktriangledown$, time rate of change of dewetted length, $\mathrm{d}L_D/\mathrm{d}t$.

is approximately the same as observed for the experiment conducted at lower C. The main difference between the two experiments is that for high C, the movement of the contact edges and the shortening of the dewetted length begin at the same time. This may indicate that for the low C experiment, time is required for a critical surfactant concentration to be reached before the dewetted length will decrease in size. At high C, the critical surfactant levels are reached rapidly and the dewetted length quickly begins shortening. This phenomenon may be explained by the fact that in order for the downstream edge to accelerate upstream, the critical advancing contact angle must be rapidly decreased. Dussan V. & Chow (1983) assume that advancing and receding contact angles are dependent upon contact line velocity. Likewise, under
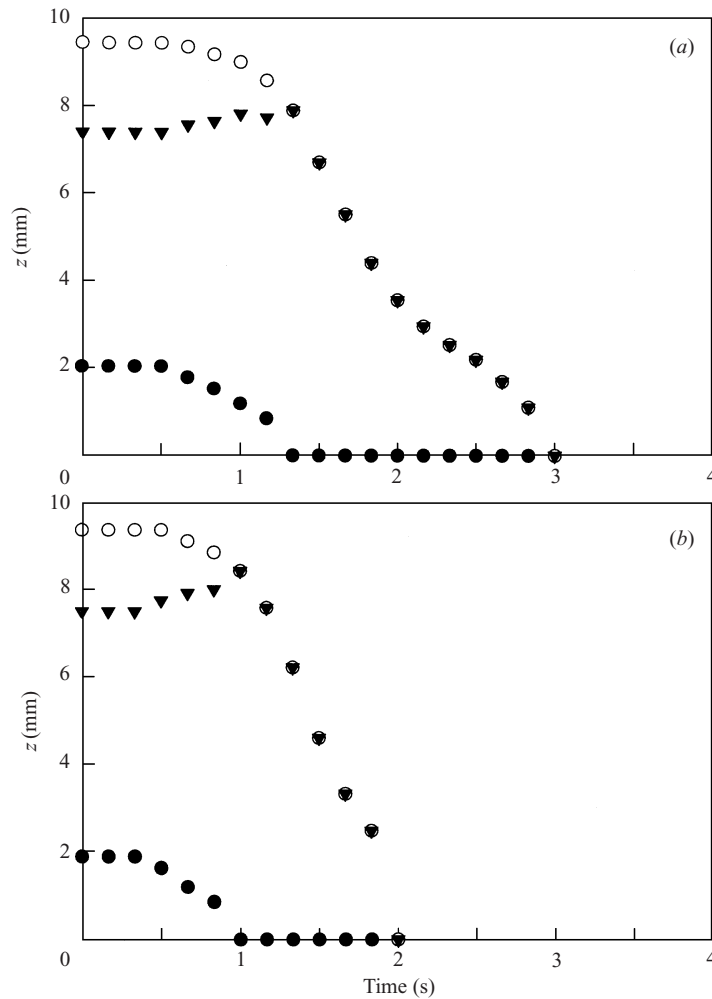
D. P. Cavanagh and D. M. Eckmann

FIGURE 18. z *vs.* time for two trials of $\omega = 45°$, $\lambda = 1.0$ and $C = 100\%$ CMC. $\bigcirc$, downstream contact edge position z_d; $\bullet$, upstream contact edge position z_u; $\blacktriangledown$, dewetted length L_D. (*a*) Trial 1. (*b*) Trial 2.

a constant force, it might also be assumed that the contact edge velocity would be dependent upon the contact angle. Whereas high C permits rapid modification of the downstream contact angle, low C will require more time, as displayed in our experiments. This behaviour was repeated in the additional trials of these parameters.

Fitting the data in figure 16 to (3) produces the corresponding velocity versus time graphs presented in figure 17. Again, we see that the upstream edge moves at a very small and nearly constant velocity. Approximately 1 s before detachment occurs, the downstream edge accelerates toward the upstream edge and the dewetted length rapidly shrinks to zero. In comparing this figure to the low C results (figure 15), we observe that the velocities of the corresponding contact edges and the rate at which the dewetted length is shortening are similar. Overall, the primary difference between the C levels is that, for high C, the time from when the effects of the surfactant are first observed to detachment is lower, indicating a more rapid effect. This would fit with greater occupancy of the interface with the surfactant, which redistributes toward the downstream edge, lowering the contact angle and permitting contact line

motion locally. Surfactant may be convected away from the upstream edge, so local conditions hardly change in that region. This difference is observed for all experiments carried out with $\lambda = 1.0$ and $\omega = 25°$, with the duration of the L_D shrinking to zero being in the range of 1–2 s.

As ω and λ are further increased beyond 25° and 1.0, respectively, the extremely dynamic nature of the current experiments becomes more apparent in the analysis of the video images acquired. Although overall qualitative repeatability of the bubble responses is observed, quantitative repeatability lessens. This is demonstrated in figure 18 where we present the contact edge positions and dewetted length as a function of time for two experiments with $\omega = 45°$, $\lambda = 1.0$, and $C = 100\%$ CMC. In both experiments, the initial dewetted length is approximately 7.5 mm and the same detachment behaviour is observed. As the surfactants adsorb to the interface, the dewetted length actually increases slightly as the upstream edge moves upstream. Eventually, the upstream edge becomes pinned on the tube wall and displays no additional movement through detachment. While $U_u = 0$, the downstream edge accelerates, briefly slows, and then accelerates again until the bubble is detached. This behaviour may be explained by the complex interaction of the surfactant transport mechanics, the bulk fluid mechanics, and the deformation of the air–water interface. As the bubble bulges upstream, the air–water interface dilates, which would tend to redistribute the surfactant on the interface, thereby lessening the effect of the SDS on the advancing contact angle. With increasing time, more surfactant is delivered to the rear of the bubble. This reduces the advancing contact angle again, permitting the downstream edge to accelerate.

4. Conclusions

In this investigation, we have revealed the extremely complex dynamic phenomena associated with the infusion of a soluble anionic surfactant into a bulk fluid containing a stationary dewetted bubble. The forces involved in the overall force balance are the buoyancy force of the bubble, the flow derived drag forces, the interfacial forces, and the contact forces. The response of a bubble to an infused soluble surfactant is dependent upon the bubble size, λ, the tube inclination angle, ω, and the bulk surfactant concentration, C. We present the range of possible behaviours in figure 4. In response to the surfactant, bubbles may move upstream or downstream or not translate at all. Also, bubbles may detach from the tube wall or the tube may remain dewetted. Bubble response is also dependent upon whether or not the tube had dewetted before the surfactant was infused. In figure 4, we have determined a region of Fr_ω and λ for which bubbles will always detach and rise when the bulk surfactant concentration is at its CMC. With C below this value, different bubble responses emerge, indicating the dynamic nature of the experiments.

Our two-dimensional analysis of the length of the dewetted region demonstrates the effects of surfactants on the velocities of the contact edges (figures 15 and 17). As the bubbles in these experiments are held stationary at the minimum flow possible, the contact edges are on the verge of moving, prior to surfactant adsorption. The infused surfactants modify the critical advancing and receding contact angles, thereby enhancing the movement of the downstream edge while impeding the movement of the upstream edge. This phenomenon is partly responsible for the detachment of bubbles from the tube wall for certain experimental conditions.

The infused surfactants have also been shown to affect the mobility of the air–water interface, as in the experiments where non-dewetted bubbles translated downstream

after surfactant exposure (figure 5*c*). Based upon insight from past investigations, this behaviour can be attributed to the development of Marangoni stresses on the interface that increase the drag of the bubble. Additionally, we have observed evidence of interfacial remobilization under certain experimental conditions where bubbles first undergo downstream translation followed by a sudden transition to upstream acceleration (figures 5*e* and 11). Evaluation of the relevant dimensionless parameters, *Bi* and *k*, reveals that remobilisation is probable in these experiments.

A mechanism for bubble detachment was put forth in the previous section in order to provide an initial explanation for the extremely dynamic process of dewetting and bubble detachment. Without knowing the exact fluid mechanics, surfactant transport mechanics and surfactant interfacial distributions, an explanation for this behaviour can only be hypothesized. We do believe, however, that the physics behind the behaviours we have categorized reveals the importance of interfacial dilation and remobilization, surfactant transport from the bulk and on the surface, and surfactant mediation of the contact angle.

REFERENCES

BLACKMORE, B., LI, D. & GAO, J. 2001 Detachment of bubbles in slit microchannels by shearing flow. *J. Colloid Interface Sci.* **241**, 514–520.

BORHAN, A. & MAO, C. F. 1992 Effect of surfactants on the motion of drops through circular tubes. *Phys. Fluids* A **4**, 2628–2632.

BRANGER, A. B. & ECKMANN, D. M. 1999 Theoretical and experimental intravascular gas embolism absorption dynamics. *J. Appl. Physiol.* **87**, 1287–1295.

BRANGER, A. B. & ECKMANN, D. M. 2002 Accelerated arteriolar gas embolism reabsorption by an exogenous surfactant. *Anesthesiology* **94**, 971–979.

CAVANAGH, D. P. & ECKMANN, D. M. 1999 Interfacial dynamics of stationary gas bubble in flows in inclined tubes. *J. Fluid Mech.* **398**, 225–244.

CHANG, C. H. & FRANSES, E. I. 1995 Adsorption dynamics of surfactants at the air/water interface: a critical review of mathematical models, data, and mechanisms. *Colloids Surfaces* A: *Physicochem. Engng Aspects* **100**, 1–45.

CHEN, J. & STEBE, K. J. 1996 Marangoni retardation of the terminal velocity of a settling drop: the role of surfactant physico-chemistry. *J. Colloid Interface Sci.* **178**, 144–155.

CHEN, J. & STEBE, K. J. 1997 Surfactant-induced retardation of the thermocapillary migration of a droplet. *J. Fluid Mech.* **340**, 35–59.

DAVIS, R. E. & ACRIVOS, A. 1966 The influence of surfactants on the creeping motion of bubbles. *Chem. Engng Sci.* **21**, 681–685.

DEBISSCHOP, K. M., MIKSIS, M. J. & ECKMANN, D. M. 2002 Bubble rise in an inclined channel. *Phys. Fluids* **14**, 93–106.

DIMITRAKOPOULOS, P. & HIGDON, J. J. L. 1997 Displacement of fluid droplets from solid surfaces in low-Reynolds-number shear flows. *J. Fluid Mech.* **336**, 351–378.

DIMITRAKOPOULOS, P. & HIGDON, J. J. L. 1998 On the displacement of three-dimensional fluid droplets from solid surfaces in low-Reynolds-number shear flows. *J. Fluid Mech.* **377**, 189–222.

DURBIN, P. A. 1988 Free-streamline analysis of deformation and dislodging by wind force of drops on a surface. *Phys. Fluids* **31**, 43–48.

DUSSAN V., E. B. 1985 On the ability of drops or bubbles to stick to non-horizontal surfaces of solids. Part 2. Small drops or bubbles having contact angles of arbitrary size. *J. Fluid Mech.* **151**, 1–20.

DUSSAN V., E. B. 1987 On the ability of drops to stick to surfaces of solids. Part 3. The influences of the motion of the surrounding fluid on dislodging drops. *J. Fluid Mech.* **174**, 381–397.

DUSSAN V., E. B. & CHOW R. T.-P. 1983 On the ability of drops or bubbles to stick to non-horizontal surfaces or solids. *J. Fluid Mech.* **137**, 1–29.

ECKMANN, D. M., CAVANAGH, D. P. & BRANGER, A. B. 2001 Wetting characteristics of aqueous surfactant-laden drops. *J. Colloid Interface Sci.* **242**, 386–394.

FDHILA, R. B. & DUINEVELD, P. C. 1996 The effect of surfactant on the rise of a spherical bubble at high Reynolds and Péclet numbers. *Phys. Fluids* **8**, 310–321.

FENG, J. Q. & BASARAN, O. A. 1994 Shear flow over a translationally symmetric cylindrical bubbles pinned on a slot in a plane wall. *J. Fluid Mech.* **275**, 351–378.

FLUMERFELT, R. W. 1980 Effects of dynamic interfacial properties on drop deformation and orientation in shear and extensional flow fields. *J. Colloid Interface Sci.* **76**, 330–349.

FURMIDGE, C. G. L. 1962 Studies at phase interfaces. I. The sliding of liquid drops on solid surfaces and a theory for spray retention. *J. Colloid Sci.* **17**, 309–324.

HE, Z., DAGAN, Z. & MALDARELLI, C. 1991 The influence of surfactant absorption on the motion of a fluid sphere in a tube. Part 1. Uniform retardation controlled by sorption kinetics. *J. Fluid Mech.* **222**, 1–32.

ILIEV, S. D. 1997 Static drops on an inclined plane: equilibrium modeling and numerical analysis. *J. Colloid Interface Sci.* **194**, 287–300.

JOHNSON, R. A. & BORHAN, A. 1999 Effect of insoluble surfactants on the pressure-driven motion of a drop in a tube in the limit of high surface coverage. *J. Colloid Interface Sci.* **218**, 184–200.

JOHNSON, R. A. & BORHAN, A. 2000 Stability of the shape of a surfactant laden drop translating at low Reynolds number. *Phys. Fluids* **12**, 773–784.

LEVAN, M. D. & NEWMAN, J. 1976 The effect of surfactant on the terminal and interfacial velocities of a bubble or drop. *AIChE J.* **22**, 695–701.

LEVICH, V. G. 1962 *Physicochemical Hydrodynamics*. Prentice–Hall.

LI, X. & POZRIKIDIS, C. 1996 Shear flow over a liquid drop adhering to a solid surface. *J. Fluid Mech.* **307**, 167–190.

LIAO, Y. & MCLAUGHLIN, J. B. 2000 Bubble motion in aqueous surfactant solutions. *J. Colloid Interface Sci.* **224**, 297–310.

MAXWORTHY, T. 1991 Bubble rise under an inclined plate. *J. Fluid Mech.* **229**, 659–673.

MYSELS, K. J. 1986 Surface tension of solutions of pure sodium dodecyl sulfate. *Langmuir* **2**, 423–428.

MILINAZZO, F. & SHINBROT, M. 1988 A numerical study of a drop on a vertical wall. *J. Colloid Interface Sci.* **121**, 254–264.

OGUZ, H. N. & SADHAL, S. S. 1988 Effects of soluble and insoluble surfactants on the motion of drops. *J. Fluid Mech.* **194**, 563–579.

PARK, C. W. 1992 Influence of soluble surfactants on the motion of a finite bubble in a capillary tube. *Phys. Fluids* A **4**, 2335–2338.

PAWAR, Y. & STEBE, K. J. 1996 Marangoni effects on drop deformation in an extensional flow: the role of surfactant physical chemistry. I. Insoluble surfactants. *Phys. Fluids* **8**, 1738–1751.

PHILLIPS, W. J., GRAVES, R. W. & FLUMERFELT, R. W. 1980 Experimental studies of drop dynamics in shear fields: role of dynamic interfacial effects. *J. Colloid Interface Sci.* **76**, 350–370.

SCHLEIZER, A. D. & BONNECAZE, R. T. 1999 Displacement of a two-dimensional immiscible droplet adhering to a wall in shear and pressure-driven flows. *J. Fluid Mech.* **383**, 29–54.

STEBE, K. J., LIN, S. Y. & MALDARELLI, C. 1991 Remobilizing surfactant retarded fluid particle interfaces. 1. Stress-free conditions at the interfaces of micellar solutions of surfactants with fast sorption kinetics. *Phys. Fluids* A **3**, 3–20.

STEBE, K. J. & MALDARELLI, C. 1994 Remobilizing surfactant retarded fluid particle interfaces. 2. Controlling the surface mobility at interface of solutions containing surface active components. *J. Colloid Interface Sci.* **163**, 177–189.

STONE, H. A. 1990 A simple derivation of the time-dependent convective–diffusion equation for surfactant transport along a deforming interface. *Phys. Fluids* A **2**, 111–112.

STONE, H. A. & LEAL, L. G. 1990 The effects of surfactants on drop deformation and breakup. *J. Fluid Mech.* **220**, 161–186.

VOLLHARDT, D. & EMRICH, G. 2000 Coadsorption of sodium dodecyl sulfate and medium-chain alcohols at the air–water interface. *Colloids Surfaces* A: *Physicochem. Engng Aspects* **161**, 173–182.

WANG, Y., PAPAGEORGIOU, D. T. & MALDARELLI, C. 1999 Increased mobility of a surfactant-retarded bubble at high bulk concentrations. *J. Fluid Mech.* **390**, 251–270.

YAMAMOTO, T. & ISHI, T. 1987 Effect of surface active materials on the drag coefficients and shapes of single large gas bubbles. *Chem. Engng Sci.* **42**, 1297–1303.

YON, S. & POZRIKIDIS, C. 1999 Deformation of a liquid drop adhering to a plane wall: significance of the drop viscosity and the effect of an insoluble surfactant. *Phys. Fluids* **11**, 1297–1308.

ZHANG, X. & BASARAN, O. A. 1995 An experimental study of dynamics of drop formation. *Phys. Fluids* **7**, 1184–1203.

ZHANG, X. & BASARAN, O. A. 1997 Dynamic surface tension effects in impact of a drop with a solid surface. *J. Colloid Interface Sci.* **187**, 166–178.

ZHANG, Y. & FINCH, J. A. 2001 A note on single bubble motion in surfactant solutions. *J. Fluid Mech.* **429**, 63–66.